

*This project has received funding from  
the European Union's Horizon 2020  
research and innovation programme  
under grant agreement No 875193*



# MODALIS<sup>2</sup>

**MODelling of Advanced LI Storage Systems**

## **REPORT ON THE NEW SIMULATION TOOLCHAIN**

This project has received funding  
from the European Union's Horizon 2020 research and innovation programme  
under **Grant Agreement No. 875193**

Deliverable number: D5.4

Due date: 31.08.2023

Nature<sup>1</sup>: R

Dissemination Level<sup>1</sup>: PU

Work Package: WP5

Lead Beneficiary: SISW

Contributing Beneficiaries:

---

<sup>1</sup> **Nature:** R = Report, P = Prototype, D = Demonstrator, O = Other  
**Dissemination level** PU = Public  
PP = Restricted to other programme participants (including the Commission Services)  
RE = Restricted to a group specified by the consortium (including the Commission Services)  
CO = Confidential, only for members of the consortium (including the Commission Services)  
Restraint UE = Classified with the classification level "Restraint UE" according to Commission Decision 2001/844 and amendments  
Confidential UE = Classified with the mention of the classification level "Confidential UE" according to Commission Decision 2001/844 and amendments  
Secret UE = Classified with the mention of the classification level "Secret UE" according to Commission Decision 2001/844 and amendments

<b>1</b>	<b>Introduction .....</b>	<b>5</b>
1.1	Purpose and Scope of the Deliverable	5
1.2	Objective of the Project Deliverable	5
1.3	Process of Development	5
1.4	Results	5
1.5	Achievements compared to Project Objectives	5
1.6	References	5
1.7	Acronyms	6
<b>2</b>	<b>Gen 3B simulation tool chain.....</b>	<b>8</b>
2.1	Gen 3B toolchain overview	8
2.2	DFT modelling	9
2.2.1	Model description	9
2.2.2	Model results	10
2.3	Particle scale modelling	11
2.3.1	Model description	12
2.3.2	Results	13
2.4	Electrode scale modelling	15
2.4.1	Electrode scale mechanical modelling description	15
2.4.2	Electrode scale mechanical modelling: results	16
2.4.3	Electrochemical and mechanical model description	18
2.4.4	Electrochemical and mechanical model results	18
2.5	Single Particle Model with Electrolyte	21
2.5.1	Single Particle Model with electrolyte description	21
2.5.2	SPM-e model results	23
2.5.3	Thermal runaway model description	25
2.5.4	Thermal runaway model results	26
2.6	3D macro-homogeneous approach	27
2.6.1	3D Cell Design in Simcenter STAR-CCM+	27
2.6.2	3D Cell Modeling approach	28
2.6.3	3D Cell Modelling results	31
<b>3</b>	<b>Gen4 simulation tool chain .....</b>	<b>33</b>
3.1	Gen4 toolchain overview	33
3.2	Atomistic modelling	34
3.3	Mesosopic scale	37
3.3.1	Dendritic growth modelling	37
3.3.2	3D mechanical modelling of the Gen4 cell	39
3.4	Single Particle Model with Electrolyte	41

**CONFIDENTIAL** until public release by the MODALIS<sup>2</sup> project consortium

3.5	3D macro-homogeneous approach	42
<b>4</b>	<b>Conclusion and Perspectives .....</b>	<b>44</b>

## Executive Summary

The goal of the MODALIS<sup>2</sup> project is to provide a comprehensive description of the behaviour of the following next generation batteries:

- Gen 3b: aiming for higher capacities for the positive and negative electrodes. The new materials used in this technology are challenging in terms of modelling due to their high volumetric expansion which will require specific new development in order to account for this phenomenon at material and cell level.
- Gen 4b: enabling the use of solid electrolytes for improved safety and to facilitate the use of Li-M for the negative electrode.

The document focuses on the description of the toolchain used for Gen 3b batteries, which is detailed in Part 2.

A total of five modeling scales were developed, ranging from ab-initio description of the Si-based active material to electrochemical modeling of cell ageing, with a focus on cooperative model design. Models were used in conjunction with experiments to elaborate anode-wide and cell-wide models of the electrochemical performance of the cell, providing additional input for some of the models involved and validating the overall project design.

First, the electronic structure and mechanical properties of the Si-based materials identified in the SiOx/C composite anode were investigated with ab-initio quantum mechanical calculations. Density Functional Theory (DFT) models were used to clarify the effect of lithiation and delithiation processes on the structure of the individual phases in the Si-based particles, and to transfer relevant data on those materials to particle level simulation.

Then, particle size model was performed to bridge the results obtained from the molecular scale model to the higher-level models. Finite Element Method (FEM) was used to predict the total volume change of the SiOx/C microparticle while considering its internal morphology and the effect of lithiation on its active and inactive materials.

At electrode scale level, the goal of the mechanical modelling performed in the project is to link the results on swelling obtained at the particle level to the electrode swelling and its impact on mechanical stability. This approach provides insights on the volume expansion of active materials for the macro scale modeling, where it plays an important role in aging mechanisms.

In order to evaluate the full cell behaviour by combining the mechanism observed at atomistic and microstructure level, a physics-based approach has been chosen consisting of a simplified electrochemical model called Single Particle Model with electrolyte (SPM-e). The model accounts for the coupling between electrochemical and mechanical processes in the anode, as well as the ageing process in the full battery cell. When compared to experimental characterization performed in the project, the model is in good agreement both for the formation process, nominal and aging behaviour. A thermal runaway model has also been developed and validated at this scale.

Finally, a detailed 3D model of the cell accounting for Solid-electrolyte interphase, lithium plating and mechanical degradation aging has been developed, in order to investigate the inhomogeneities of aging within the studied cell.

The methods and tools developed for the Gen3B cell have also been applied to a prototype Gen4 cell. The models and results are described in part 3.

# 1 Introduction

## 1.1 Purpose and Scope of the Deliverable

This report on MODALIS<sup>2</sup> report on the new simulation toolchain presents the main modeling tools used in the project to model next generation batteries from material to cell, as well as the methodologies used to pass the parameters and adapt the modeling between the scales. The report presents the models and results for the Gen 3b cell of the project, for which the complete toolchain has been implemented and validated with experimental measurements done in the project.

The developments and validations done for the Gen 4b cell are still ongoing and are not described in this document.

## 1.2 Objective of the Project Deliverable

The objective of this deliverable is to describe the various models developed for the Gen 3b cell at the different scales (material, particle, electrode, cell) as well as the main analysis and results obtained with these models.

## 1.3 Process of Development

This deliverable has been developed by Siemens based on the various deliverables, presentations, papers and technical documentation produced during the project.

## 1.4 Results

The result of this deliverable consists in a description of the modelling approaches used from material to cell level for Gen 3b, as well as the main analysis performed with these models.

## 1.5 Achievements compared to Project Objectives

For Gen 3b, a complete simulation toolchain ranging from ab-initio calculation to full cell model has been developed and validated with regard to the experiments performed during the project.

Similar models have been developed during the project for Gen 4 batteries, focusing on surface stability and lithium dynamics through solid/solid interfaces, and volumetric expansion model of cells. The validation of these models and their integration in a complete toolchain is still ongoing at the present stage.

## 1.6 References

[1] Jain, A. et al. Commentary: The materials project: A materials genome approach to accelerating materials innovation. *APL Mater.* 1, (2013).

[2] Dal Corso, A. Thermo\_PW.

- [3] Man, C. S. & Huang, M. A simple explicit formula for the Voigt-Reuss-Hill average of elastic polycrystals with arbitrary crystal and texture symmetries. *J. Elast.* 105, 29–48 (2011).
- [4] J. Newman, W. Tiedemann, Porous-electrode theory with battery applications, *AIChE J.* 21 (1975) 25–41. <https://doi.org/10.1002/aic.690210103>.
- [5] C. Liu, O. Arcelus, T. Lombardo, H. Oularbi, A.A. Franco, Towards a 3D-resolved model of Si/Graphite composite electrodes from manufacturing simulations, *J. Power Sources* 512 (2021) 230486. <https://doi.org/10.1016/j.jpowsour.2021.230486>.
- [6] T.F. Fuller, M. Doyle, J. Newman, Simulation and Optimization of the Dual Lithium Ion Insertion Cell, *J. Electrochem. Soc.* 141 (1994) 1–10. <https://doi.org/10.1149/1.2054684>.
- [7] M. Petit, E. Calas, J. Bernard, A simplified electrochemical model for modelling Li-ion batteries comprising blend and bidispersed electrodes for high power applications, *J. Power Sources* 479 (2020) 228766. <https://doi.org/10.1016/j.jpowsour.2020.228766>.
- [8] S.E.J. O’Kane, W. Ai, G. Madabattula, D. Alonso-Alvarez, R. Timms, V. Sulzer, J.S. Edge, B. Wu, G.J. Offer, M. Marinescu, Lithium-ion battery degradation: how to model it, *Physical chemistry chemical physics PCCP* 24 (2022) 7909–7922. <https://doi.org/10.1039/d2cp00417h>.
- [9] J.M. Reniers, G. Mulder, D.A. Howey, Review and Performance Comparison of Mechanical-Chemical Degradation Models for Lithium-Ion Batteries, *J. Electrochem. Soc.* 166 (2019) A3189–A3200. <https://doi.org/10.1149/2.0281914jes>.
- [10] Dai, Y. Cai, L., White, E., “Simulation and analysis of stress in a Li-ion battery with a blended LiMn<sub>2</sub>O<sub>4</sub> and LiNi<sub>0.8</sub>Co<sub>0.15</sub>Al<sub>0.05</sub>O<sub>2</sub> Cathode,” *Journal of Power Sources*, vol. 247, pp. 365–376, 2014.
- [11] E. Prada, D. Di Domenico, Y. Creff, J. Bernard, V. Sauvant-Moynot, F. Huet, A Simplified Electrochemical and Thermal Aging Model of LiFePO<sub>4</sub>-Graphite Li-ion Batteries: Power and Capacity Fade Simulations, *J. Electrochem. Soc.* 160 (2013) A616–A628. <https://doi.org/10.1149/2.053304jes>.
- [12] Chen, Lei et al. (2015) Modulation of dendritic patterns during electrodeposition: A nonlinear phase-field model. *Journal of Power Sources* 300, DOI: 10.1016/j.jpowsour.2015.09.055
- [13] Danilov, D., Niessen, R. A. H., & Notten, P. H. L. (2011). Modeling all-solid-state Li-ion batteries. *Journal of the Electrochemical Society*, 158(3), A215–A222. <https://doi.org/10.1149/1.3521414>
- [14] R. Koerver et al. *Energy Environ. Sci.* 11 (2018) 2142–2158. <https://doi.org/10.1039/C8EE00907D>.

## 1.7 Acronyms

SiO<sub>c</sub> - Silicon Oxide

NMC - Lithium Nickel Manganese Cobalt oxide

DFT - Density Functional Theory

FEM - Finite Element Modeling

AIMD - Ab-Initio Molecular Dynamics

SOC – State Of Charge

P2D - Pseudo two Dimensional

DEM - Discrete Element Method

CGMD - Coarse-Grained Molecular Dynamics

SEM – Scanning Electron Microscope

LJ - Lennard-Jones

GH - Granular-Hertzian (GH)

FFs - force fields

SOL - State of lithiation

SEI - Solid-Electrolyte Interphase

SPM-e - Single Particle Model with electrolyte

HPPC - Hybrid Pulse Power Characterization

ARC - Accelerating Rate Calorimeter

FV - Finite Volume

FE - Finite Element

LiP - Li plating

LAM - Loss of Active Material

## 2 Gen 3B simulation tool chain

### 2.1 Gen 3B toolchain overview

The first goal of the project is to provide a comprehensive description of the behaviour of the Si-based anode through its cycle life. For this reason, a total of five modeling scales were developed, ranging from ab-initio description of the Si-based active material to electrochemical modeling of cell ageing, with a focus on cooperative model design (Figure 1).

On the lower scale, ab-initio quantum mechanical calculation was used to investigate the electronic structure and mechanical properties of the Si-based materials identified in the SiOx/C composite anode.

Then, the particle size model was defined to bridge the results obtained from the molecular scale model to the higher-level models.

Microstructure modelling coupling mechanical and electrochemical behaviour was performed to investigate the electrode behaviour in realistic condition.

At cell level, using 1D cell level model enabled the evaluation of the performance and long-term behaviour of the battery.

Detailed 3D cell model was developed to provide insight on the impact of inhomogeneities inside cells.

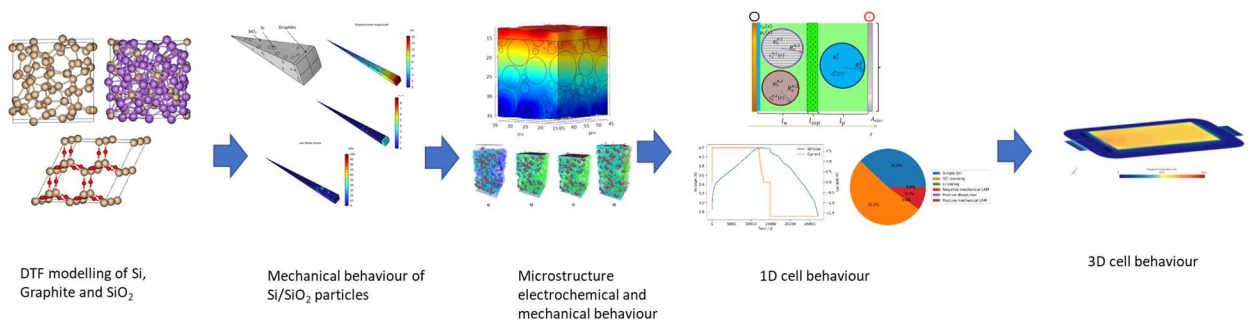


**Figure 1: Gen3B toolchain overview**

The studied cell has been designed and manufactured in the scope of H2020 MODALIS<sup>2</sup> project. The cells were manufactured using NMC811 as positive material and SiOx/C material as negative material. Then 26 positive/separators/negative assemblies (13 double coated positive and 12 double coated + 2 single coated negative) have been stacked into pouch cells to form 5 Ah cells.

## 2.2 DFT modelling

The electronic structure and mechanical properties of the Si-based materials identified in the SiO<sub>x</sub>/C composite anode were investigated with ab-initio quantum mechanical calculations.

The objective of the Density Functional Theory (DFT) models is to clarify the effect of lithiation and delithiation processes on the structure of the individual phases in the Si-based particles, and to transfer relevant data on those materials to the Finite Element Modeling (FEM) model of the particle.

### 2.2.1 Model description

Three phases could be identified experimentally in the pristine composite particle: Si and SiO<sub>2</sub> in the bulk of the particle, and graphitic C in its shell. For the oxidised matrix phase, models for SiO<sub>2</sub>, Li<sub>2</sub>O and Li<sub>4</sub>SiO<sub>4</sub> phases were investigated. Their Crystal data structure was obtained from the Materials Project website [1]. The unit cells used for (Li<sub>2</sub>O)<sub>x</sub>(SiO<sub>2</sub>)<sub>y</sub> are shown in Figure 2.

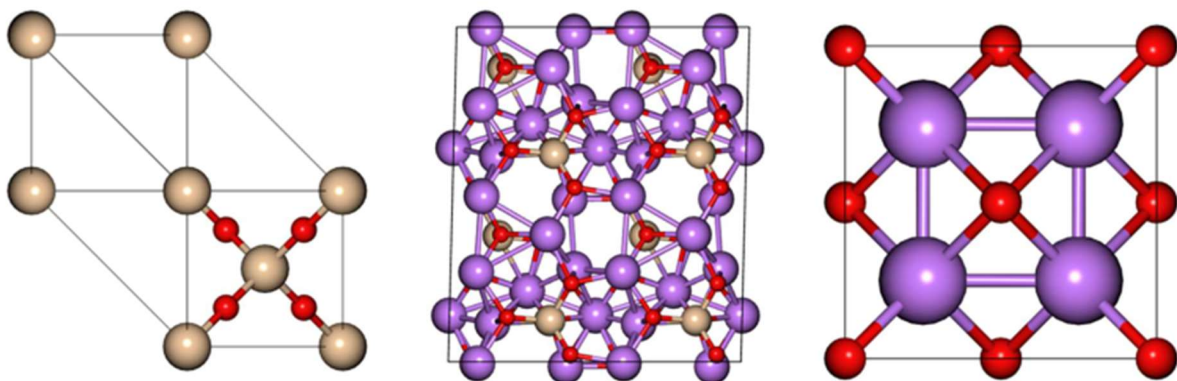


Figure 2: Unit cell structures for SiO<sub>2</sub>, Li<sub>4</sub>SiO<sub>4</sub> and Li<sub>2</sub>O (Si:brown, Li:purple, O:red).

To represent the charging (lithiation) and discharging (delithiation) processes in the anode, five amorphous Li<sub>x</sub>Si phases (Si, Li<sub>0.5</sub>Si, Li<sub>1</sub>Si, Li<sub>2</sub>Si, and Li<sub>3.75</sub>Si) were created and amorphized through ab-initio molecular dynamics (AIMD) calculations at finite temperature via a specific procedure. The unit cells used in the calculation are shown in Figure 3

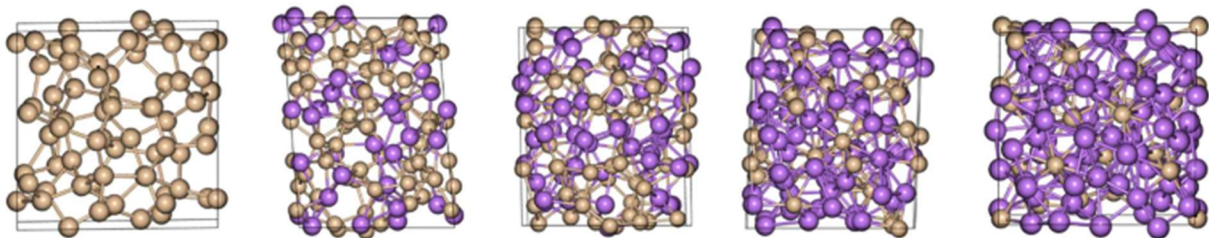


Figure 3: Final unit cell structures for, from left to right: Si, Li<sub>0.5</sub>Si, Li<sub>1</sub>Si, Li<sub>2</sub>Si, Li<sub>3.75</sub>Si (Si:brown, Li:purple).

The number of Li and Si atoms in each phase is reported in Table 1.

	Si	Li <sub>0.5</sub> Si	Li <sub>1</sub> Si	Li <sub>2</sub> Si	Li <sub>3.75</sub> Si
# of Li atoms	0	32	48	64	75
# of Si atoms	64	64	48	32	20

**Table 1: Atomic composition of LixSi phase**

## 2.2.2 Model results

### Volumetric expansion

The characteristic volumetric expansion of each material is a key parameter in several electrochemical models of lithium-ion batteries. This parameter is often difficult to obtain accurately from experiments, as the macroscopic expansion of a material can be a result of a combination of factors beyond the actual change in lattice dimension at the nanostructure, such as solid-electrolyte interphase formation and pulverization. This is generally the case for Si-based anodes, and particularly for the SiOx/C material, due to its composite nature and difficult characterization operation.

Experimental parameters are often only available for pristine and fully lithiated materials, resulting in a linear interpolation of the expansion versus the lithium concentration; Figure 4 shows how this approximation is far from the actual behaviour of the LixSi active anode material, significantly overestimating the contribution of low and medium Li concentrations and modifying the expected behaviour of Si-based anodes in mechanical models. The investigation of intermediate phases, instead, provided additional data facilitating a more accurate representation of the material's behaviour.

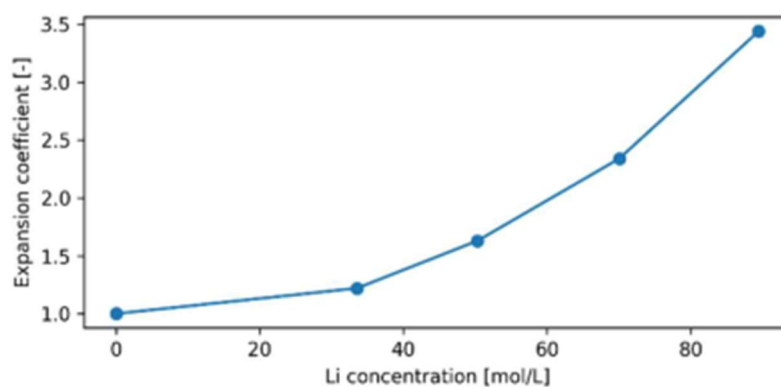


**Figure 4: Nonlinear dependency of the volumetric expansion with the Li concentration in LixSi.**

### Mechanical properties

This amorphized unit cells were used for the calculation of the mechanical properties of all phases of the Si/C anodic particle as a function of the state of charge via the Thermo\_PW software [2]. Each phase was subjected to a series of 6 successive compressions and extensions in various

directions and the total electronic energies of each strained phase was recorded through a standard DFT calculation. A polynomial fit of the DFT energies resulted in an elastic tensor for each phase. Finally, Bulk modulus, Young's modulus, and Poisson ratio approximation were calculated for all phases through the Voigt [3] model of uniform distribution of strain and Reuss model of uniform distribution of stress.

The plot of the Bulk modulus of Si against the lithium molar fraction (Figure 5) shows the strong changes in mechanical properties happening in the anode during the charge and discharge processes; as Si is transformed into Li<sub>2</sub>Si its resistance to compressive stress is halved, and then again reduced by approximately 20% as the lithium content is increased to Li<sub>3.75</sub>Si. Similar trends are also found for the Shear and Young moduli, which also decrease near-linearly with lithium concentration.

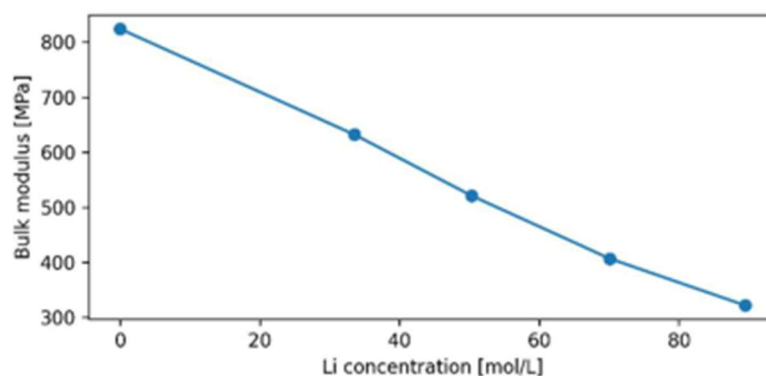


**Figure 5: Bulk modulus (in kbar) of LixSi phases vs. their Li molar fraction.**

In this chapter we presented the ab-initio investigation of LixSi and (Li<sub>2</sub>O)<sub>x</sub>(SiO<sub>2</sub>)<sub>y</sub> materials and the data which it could provide for the overall multiscale project. The AIMD simulation of LixSi phases and the ab-initio calculation of the elastic properties of the SiO<sub>x</sub> material provide valuable insight on the chemical properties of these phases during the lithiation and delithiation processes, highlighting the importance of the mechanical properties to explain the chemical changes of the material which have been highlighted experimentally, as well as providing quantitative data for the volumetric and elastic properties as a function of the lithium content. The data, which would have been impossible to obtain experimentally with such precision, can be used in the mechanical modelling presented in the following chapter.

## 2.3 Particle scale modelling

The particle size model is defined to bridge the results obtained from the molecular scale model to the higher-level models. The experimental characterization and the DFT investigation reported in the sections above provide a clear picture of the ideal microscale morphology of the SiO<sub>x</sub>/C anodic material. For the most part, the material is composed of relatively homogeneous graphite-

based particles, and of smaller composite SiO<sub>x</sub>/C particles, both of which contribute to the overall performances of the material. While the morphology of the graphitic particles is trivial, that of the Si-based particle was deemed worthy of a specific investigation, in order to translate the volumetric expansion dataset obtained from DFT modelling to electrode-scale models of the material's mechanical performances.

### 2.3.1 Model description

Finite Element Method (FEM) were performed in COMSOL Multiphysics to predict the total volume change of the SiO<sub>x</sub>/C microparticle while considering its internal morphology and the effect of lithiation on its active and inactive materials. For the sake of simplicity, the simulations were performed neglecting the initial conditioning cycles and any subsequent ageing phenomenon, i.e. considering the microparticles under regular operating conditions.

Five replicas of the simulation model were generated to match five conversion rates of SiO<sub>2</sub> in Si, Li<sub>2</sub>O, and Li<sub>4</sub>SiO<sub>4</sub>. The effects of lithiation on the active phases within the particle (C and Si) are modelled dynamically, while the impact of the inactive phase (SiO<sub>2</sub>) on the microparticle deformation is assessed via steady-state simulations. The amorphous Si clusters were represented by a percolation nanospheres surrounded by a homogeneous matrix with variable composition. The particle core was enclosed in a shell of graphite. The mechanical properties of the homogeneous matrix were evaluated by averaging the properties of its constituents (namely, Si, Li<sub>2</sub>O, and Li<sub>4</sub>SiO<sub>4</sub>) weighted by their molar fractions. To reduce the computational cost, the simulation domain was generated exploiting the system symmetry: a spherical wedge was considered sufficiently representative of the structure, transport properties, and mechanical behaviour of the whole microparticle, while its reduced volume compared to the whole spherical particle allowed for more practical computational loads.

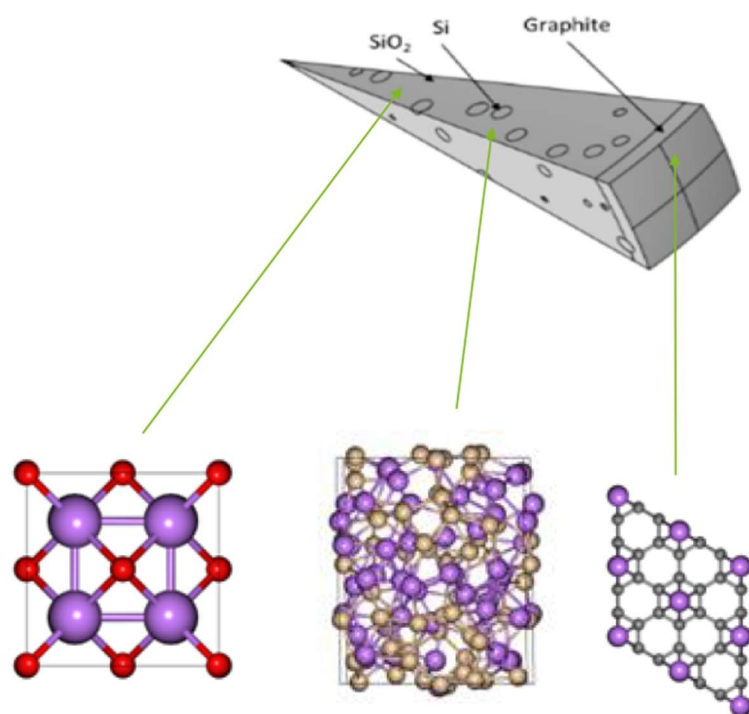


Figure 6: Representation of the spherical wedge used to perform the mechanical simulations. (Si:brown, Li:purple, O:red)

## 2.3.2 Results

### Lithium diffusion modelling

The diffusion of lithium within the microparticle was modelled using a simplified one-dimensional model. The present modelling approach assumes that lithium can only diffuse in the outer graphite shell and through the silicon clusters, neglecting lithium transport through the multicomponent matrix. The microparticle core was therefore assumed to behave as a porous medium, with lithium diffusing only through the silicon percolation. Besides the initial silicon volume fraction, the main geometric parameter influencing this process is the aggregate tortuosity, which can be interpreted as the ratio between the length of the average path required by lithium to cross the particle core and the shortest possible path, namely a straight radial line. Diffusion behaviour and consecutive concentration profiles were used with the material swelling behaviour described in 2.2.2 to evaluate the swelling behaviour of composite particles used in the cells.

### Mechanical strain in the SiO<sub>x</sub>/C particle

To retrieve the microparticle expansion curves as a function of the SOC, 15 different concentration distributions were considered for each conversion rate considered. Since lithium diffuses only in the silicon clusters and in the outer graphite shell, the internal structure of the microparticles is progressively altered by the intercalation strain, resulting in a compression of the multicomponent

matrix, an increase in the volume fraction of the Si clusters, and a progressive change in both the internal and external radii (Figure 7)

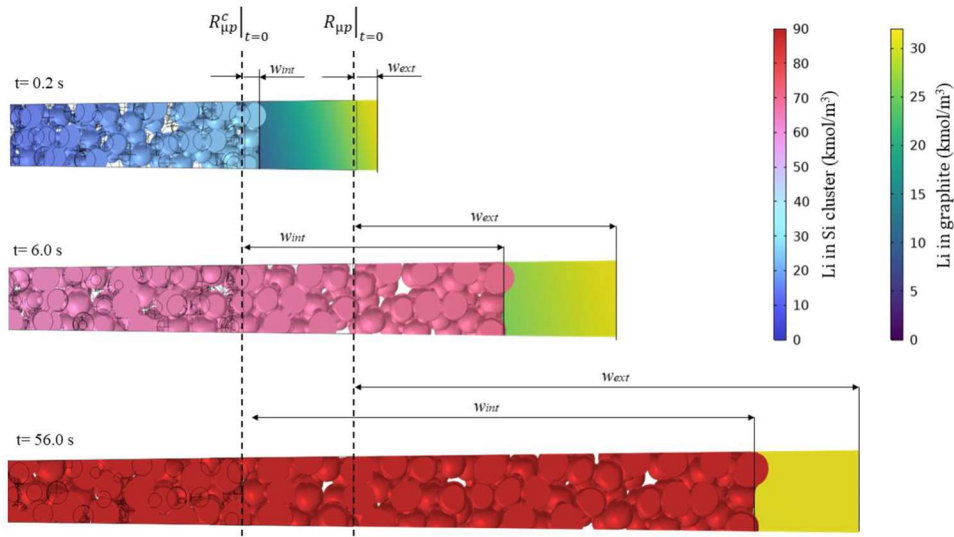


**Figure 7: Intercalation-driven deformation.** The progressive increase in Li concentration in graphite and silicon clusters forces the inner and outer shell radii to expand. The figure refers to the configuration with a 0% conversion rate.

Then several assumptions were made in order to account the whole swelling behaviour of the particles depending on the conversion of silicon oxide into Li silicate or lithiated silicon. Those assumptions could lead to various outcomes regarding the material specific capacity as well as its swelling. The higher the SiOx is converted to cyclable material the higher the specific capacity of the material and the higher its swelling. From experiments, a specific capacity of the Si-based particles was found (750 mAh/g) from which a specific correlation was deduced assessing the particle volume variation as a function of its state of charge (Figure 8)

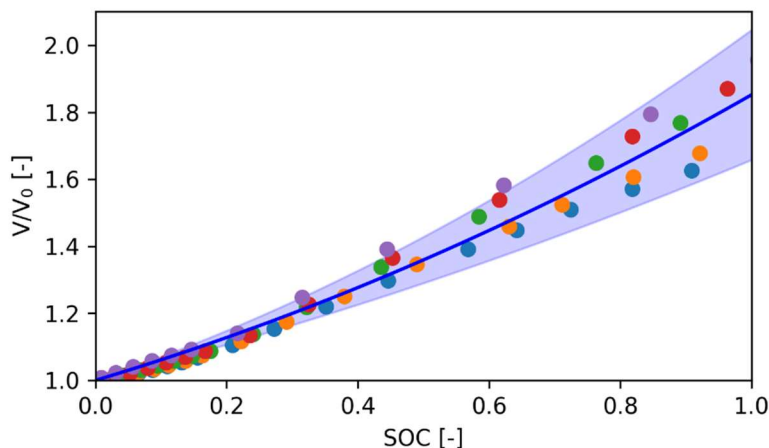


**Figure 8: Particle volume variation as a function of SOC with several conversion assumptions and 1 specific capacity measurement.**

The obtained correlation has been used further in electrode scale and cell scale modelling.

## 2.4 Electrode scale modelling

The volume expansion of silicon particles plays an important role in silicon-based composite electrode performance, used in the next-generation battery design. This volume expansion results in microstructural changes, which influence the thickness of the electrode, the interfacial contact area, and potentially the mechanical aging mechanisms. Needing a better understanding of the electrochemical and mechanical behaviour of silicon particles at the mesoscale level is fundamental.

Because of the heterogeneous distribution nature of the electrode particles in the C/SiO<sub>x</sub> electrode, the classical macroscopic P2D model is not sufficient to capture all the mesoscale phenomena [4]. Therefore, 3D computational modeling has become an efficient tool to bring insights into these domains [5]. One of the key elements to guarantee the accuracy and robustness of these mesoscale electrode models is the porosity and tortuosity of microstructure.

Experimental technology such as X-ray tomography has been used recently to extract the exact microstructure of active materials and binders and, by using SEM imaging, the microstructure-resolved mesh can be built for further 3D physical-based model usage. However, such approaches are too expensive to use regularly, and they are not suitable for a fast battery design environment.

In our project, Discrete Element Method (DEM) reconstruction approach, where the microstructural features of electrodes may be replicated in the simulation by establishing a bond-contact model based on the Hertz contact model, has been selected because of its simplicity and efficiency to obtain the particles coordinates.

### 2.4.1 Electrode scale mechanical modelling description

The goal of the electrode scale mechanical modelling is to link the results on swelling obtained at the particle level described in the previous section to the electrode swelling and its impact on mechanical stability.

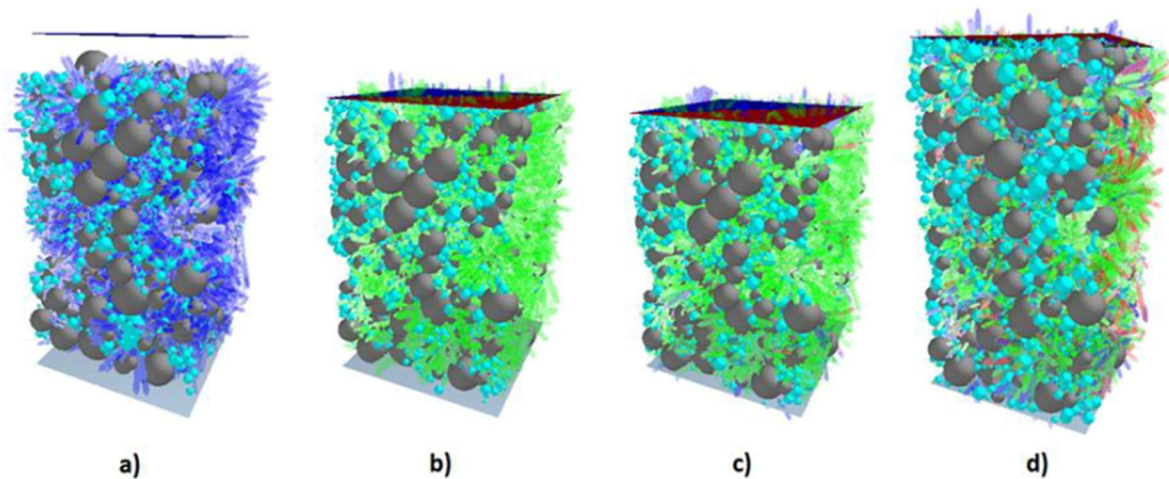
The negative electrode models have two objectives regarding the optimization of battery durability. The first is to predict anode swelling as a function of applied pressure, to evaluate the impact of swelling on the stack's other components. Then, by analysing structural changes in the material, the impact of various factors on binder damage can be assessed.

Particles are generated in a simulation box, with periodic boundaries in direction x and y to represent a seemingly infinite electrode plane. Grain distribution emulates the particle size distribution measured on the active material, and is divided in two populations, "graphite" and "silicon oxide" which vary by their size distribution and swelling properties. Size distributions are based on microstructural analysis from experiments. The grain assembly is compressed between two

plates in the z direction to a target thickness corresponding to practical electrode thickness. The grains are left to dissipate their kinetic energy before bonds are created between the sufficiently closed particles. After the bonds are created, a stress constraint is applied to the top plate to simulate the effect of confinement. Once the system has stabilized, swelling simulation is done by progressively modifying the particle diameters.

### 2.4.2 Electrode scale mechanical modelling: results

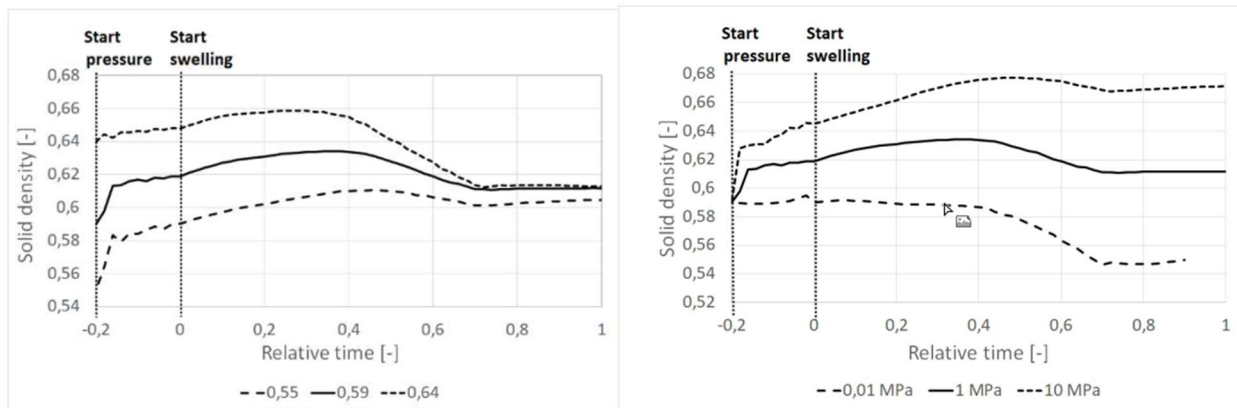
The main outputs of the simulation are the swelling at electrode level and the binder damage. Swelling gives information on the competition between macroscopic electrode swelling and porosity resorption and provide input on porosity evolution and its potential impact on electrolyte access to active material. Binder damage is not accessible to direct observation but is of key interest to predict cyclability of the electrode as it correlates directly to particle electric isolation.



**Figure 9: Evolution of the simulated negative electrode material (Graphite: grey, silicon Oxide: light blue, unbounded contacts: blue, intact bounds: green, broken bounds: red)**

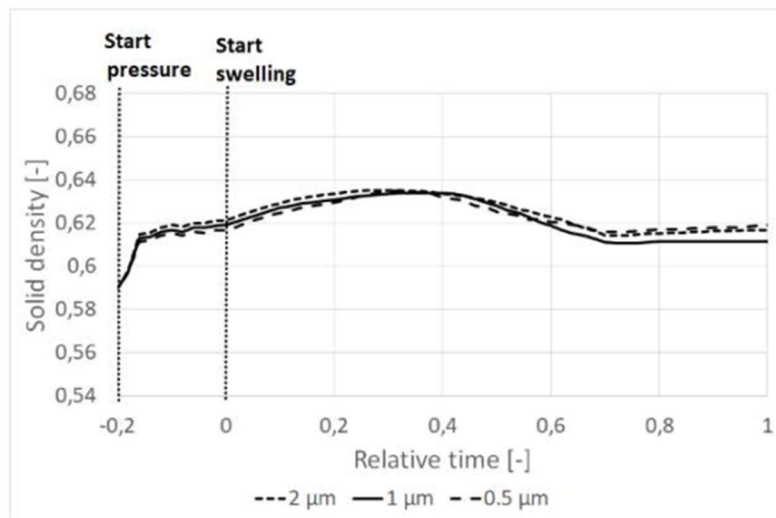
**a) particle beds just after generation b) at the end of the end of the compression phase to target density c) after application of the 1 MPa pressure and stabilization d) at the end of the swelling procedure**

Figure 10 displays the evolution of density during the swelling, for varying starting density. The density of the system follows complex evolution but with a trend to eventually converge to a final density independently of the starting density. This final density was observed to be dependent of confining pressure. The result is important as it implies that targeting important initial porosity to allow for good electrolyte circulation might not be effective in case of important swelling and counter-pressure during cycling.



**Figure 10: Evolution of density during swelling**

Concerning binder properties, such as elongation at breakage, they were observed to have no influence on the evolution of particle density (Figure 11). The results can be understood in the light of the large contrast of stiffness between mineral active particles and the polymer binder. The swelling of the particles generates important contacts efforts on the active particles, sufficient to overcome the stress generated by the bonds. The evolution of the grain assembly topology is then totally piloted by geometrical constraints on grains, and not the bonds properties.



**Figure 11: impact of binder properties on particle density**

As a conclusion, particle arrangement, including density, is mostly unaffected by the presence of the binder. Binder is not stiff enough to generate sufficient stress to influence the behaviour of the assembly, which is piloted by geometrical properties such as initial packing, or maximum density for a given granulometry. From the point of view of binder resistance, particle relative movement can be considered as a boundary condition, generating forced strains that the binder network may or may not accommodate without breaking, depending on its elastic and breakage properties. This uncoupling is an important result for the understanding of the behaviour of such systems, to be considered in larger scales modelling approaches.

### 2.4.3 Electrochemical and mechanical model description

The electrochemical model of the half-cell electrode is implemented in COMSOL Multiphysics. The model is based on the Doyle-Fuller-Newman model [4][6]. It is composed of a set of equations established on concentrated solution theory and porous electrode theory, which describes transport in the active material phase and the electrolyte. In addition to the electrochemical and transport equations, a mechanical model is added to describe the swelling of the Si-based particles, which is coupled with the output of the electrochemical model. Due to the complexity of Si-based particle inner microstructure, the stress generated between silicon and silicon oxide is not considered in this scale of the model. The effective mechanical parameters such as the Poisson ratio and Young Modulus are the output from the particle-scale model described in the previous section.

### 2.4.4 Electrochemical and mechanical model results

A half-cell is simulated by taking graphite particles and Si-based particles as a reconstructed cathode with an ideal metallic lithium anode, the aim is on the one hand to better understand the relationship between microstructure and performance, and on other hand to provide insights for the macro scale model. The half-cell is discharged at 1C with a cut-off potential at 0.001V. The simulation is carried out by considering an isothermal environment.

Figure 12 shows the State of lithiation (SOL) of Si-based particles and graphite particles at a different discharging time: 0.1h, 0.3h, and 0.5h. Overall, two active materials undergo different paths for lithiation. At the beginning of the discharge, the graphite particles dominate the mass transfer at the interface, resulting in a much higher SOL compared to Si-based particles. After reaching the middle of discharge, the Si-based particles start to dominate. The reason behind this behaviour is a combination of different aspects, such as the heterogeneity of overpotential, the active reaction surface and the speed of particles swelling, etc. The heterogeneity of SOL between Si-based particles and graphite particles is clear thanks to the 3D view. Depending on the spatial location of the particle, the SOL can be very different for graphite particles, but rather more uniform for Si-based particles.

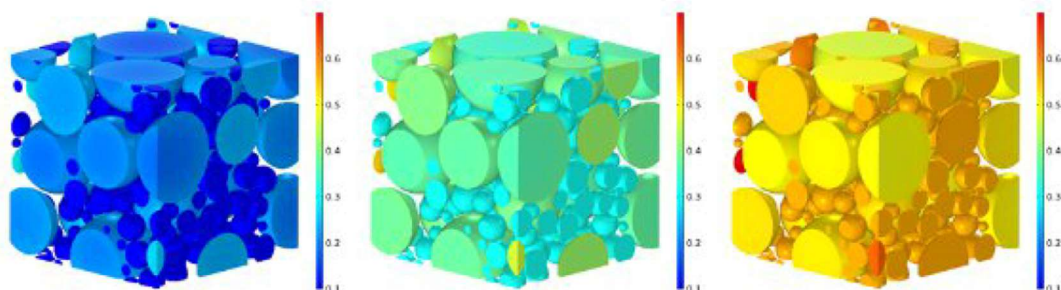


**Figure 12: State of lithiation (SOL) at 0.1h, 0.3h, and 0.5h (from left to right)**

Figure 13 shows the heterogeneous local current densities at both active materials. The color legend is set up differently to distinguish the two materials. The same type of behavior is observed

again, where graphite dominates the electrochemical reaction at the interface, resulting in a higher current density at the beginning of discharge. Si-based particles, later on, take the upper hand.

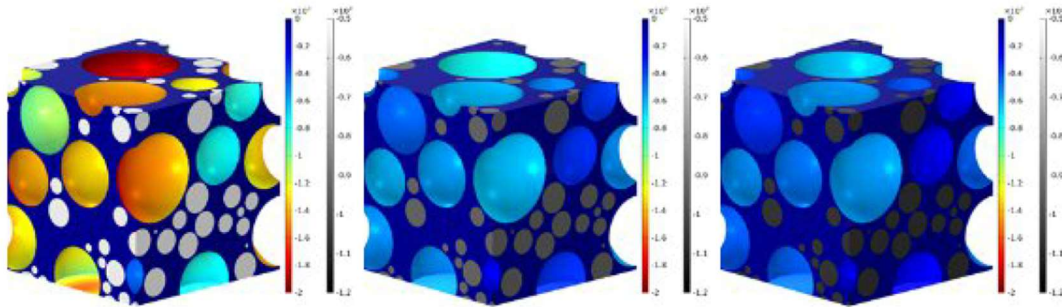


**Figure 13: Local current density (mA/m<sup>2</sup>) of graphite and Si-based particles at 0.1h, 0.3h, and 0.5h (from left to right)**

Concerning the mechanical side, the swelling of Si-based particles during lithiation is significant (up to 300%) compared with the graphite particles (10%). These volume expansions can generate enormous stress in active material and in binders, which may cause cracks, Solid-Electrolyte Interphase (SEI) formation, binder detachment, and other types of damage to the composite electrode. Therefore, it is interesting to understand the heterogeneous stress distribution via 3D microscale modeling, which is highly dependent on the size of active material and the mechanical properties of the material.

The volume expansion of Si-base particles is highly dependent the partial molar volume of lithium. Based on the particle scale simulations carried out in previous section, the effective partial molar volume of Si-based particles is calculated based on volumetric strain. Three curves of different values of  $\text{Li}_x\text{Si}_y$  are showed in Figure 14, where the value is evaluated by the state of charge of lithium in Si-base particle

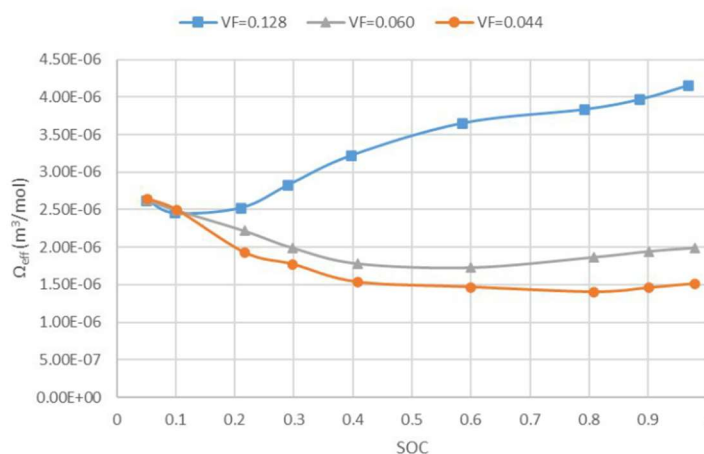


**Figure 14: Partial molar volume of lithium in Si-base particles under different volume fraction of  $\text{Li}_x\text{Si}_y$  equals to 0.044, 0.060 and 0.128**

Three simulations are carried out with the different values of which are computed from particle scale simulation, to investigate its impact. The volume expansion of the composite electrode is proportional to the value of as illustrated in Figure 15. When the volume fraction of  $\text{Li}_x\text{Si}_y$  equals to 0.128, the volume expansion ratio of Si-based particles can reach nearly 1.07, considering this composite anode has around only 22wt% of silicon.

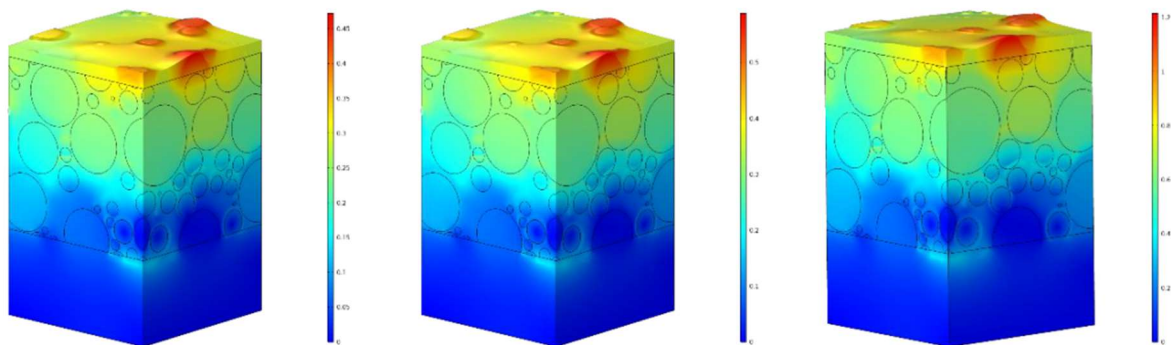


**Figure 15: Displacement ( $\mu\text{m}$ ) of composite electrode with under volume fraction of  $\text{Li}_x\text{Si}_y$  equals to 0.044, 0.060 and 0.128**

Figure 16 shows the pressure endured in the binder-electrolyte domain with different values of due to the expansion of active materials. It is logical to see a combination of negative and positive values, which indicates the domain is suffered from contractions and compressions. These opposing interactions can cause distinct degradation mechanisms, such as electrode structural integrity deterioration and binder separation from active materials particles. The higher the value of is, the more mechanical degradation that the binder-electrolyte domain endured.

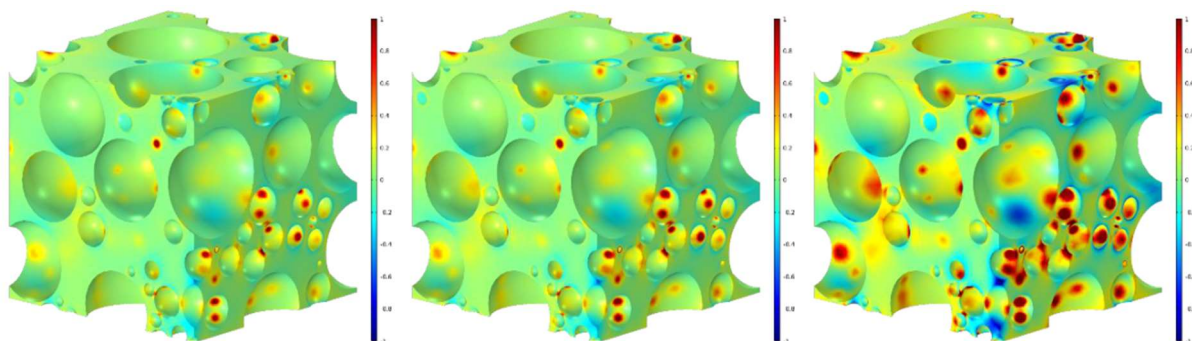


**Figure 16: Pressure (GPa) endured in binder-electrolyte with under volume fraction of  $\text{Li}_x\text{Si}_y$  equals to 0.044, 0.060 and 0.128**

The current approach is mechanical part aims to provide insights on the volume expansion of active materials for the macro scale modelling, where it plays an important role in aging mechanisms. To evaluate the full cell behaviour by combining the observed atomistic and microstructure

level mechanism a physics-based approach has been chosen consisting in a Single Particle Model with electrolyte which is presented below.

## 2.5 Single Particle Model with Electrolyte

In order to evaluate the full cell behaviour by combining the mechanism observed at atomistic and microstructure level, a physics-based approach has been chosen consisting of a simplified electrochemical model called Single Particle Model with electrolyte (SPM-e), has described in [7]. The model accounts for the coupling between electrochemical and mechanical processes in the anode, as well as the ageing process in the full battery cell.

### 2.5.1 Single Particle Model with electrolyte description

The model accounts for main mechanisms occurring in the battery such as solid and liquid diffusion, electrochemical kinetics, solid and liquid charge balance and coupled thermal effects. In this case, The positive electrode only comprises 1 material which is NMC811 whereas the negative electrode is composed by graphite and SiO<sub>x</sub>(Figure 17). Due to the expected impact of mechanical stresses, mechanical effects have been added in the diffusion mechanisms and aging mechanisms accounting for mechanics have been added.

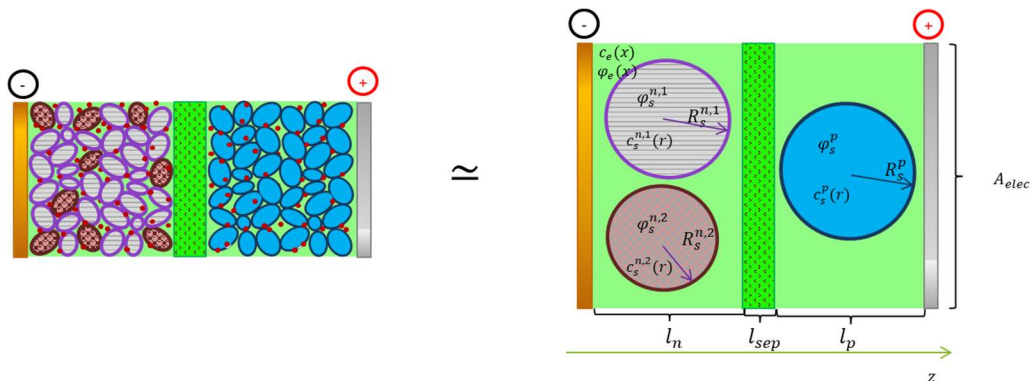


Figure 17: Single Particle Model with electrolyte (SPM-e)

### Mechanical modeling

As concentration gradients are developing into the particles, hydrostatic stresses within the spherical particles can be evaluated based on thermal expansion analogy [10]. The diffusion flux in the electrochemical model is modified in order to account for this hydrostatic stress.

Due to material swelling, the whole electrode composite is subject to swelling leading to global swelling of the battery. As demonstrated thanks to DEM approach, the electrode swelling is directly given by the individual swelling of materials. This swelling leads to compression of other

materials such as separator or packaging which act as springs. Spring models has been integrated in the SPM-e model, and the springs displacements are evaluated through the volumetric swelling of the electrodes.

### **Aging modeling**

To account for most aging mechanisms especially the mechanical effects on aging mechanisms, main state of the art mechanisms have been accounted for and integrated into the modelling [8][9]. Generic approaches have been chosen in order to easily fit few model parameters to previously obtained results while keeping relevant physical behaviours. The aging mechanism implemented are:

- **Solid-Electrolyte Interphase (SEI) formation**

Solid-Electrolyte Interphase (SEI) formation is one of the major mechanisms leading to performance degradation in Li-ion batteries. In this mechanism, an interphase layer is created by the reduction of solvent molecules at the negative electrode interface creating the SEI layer. Solvent diffuses from the SEI/electrolyte interface until the SEI/active material interface. Thus this phenomenon is limited by diffusion in the formed SEI layer as well electrochemical kinetics [11]. In order to reduce this model complexity, the convection of solvent due to SEI layer movement is neglected. The impacts of SEI layer formation are:

- A parasitic current leading to Li deintercalation from the negative electrode or loss of lithium inventory
- Creation of a resistive layer leading to power fade
- Clogging of electrode porosity

- **Lithium plating**

As negative electrode goes below 0V versus Li<sup>+</sup>/Li potential, metal lithium can be directly deposited on the negative electrode leading to potential dendrite formation and sometimes short-circuits. During subsequent discharge, this same metallic lithium can be oxidized to Li<sup>+</sup> leading to its recovery. Part of this lithium is trapped due to SEI formation on the newly formed interface or from contact losses. As a consequence, in our simplified approach, a Li deposition parasitic current is computed and only a fraction of it is accounted for in the final charge balance to represent the recovery of deposited lithium.

- **Loss of active material due to electrode oxidation**

On the positive electrode, high potential lead to instability of the electrolyte with the positive active material. A parasitic reaction occurs leading to electrolyte oxidation and active material losses. In this case, the reaction will impact the active material mass fraction which is reduced due to this reaction. Due to the oxidation reaction, there are both loss of Li inventory, and loss of active material which is represented by the decrease of positive active material volume fraction decrease.

- **Stress induced aging**

As discussed in the previous section, mechanical stresses have an impact on the long-term performances of Si based anodes. At particle level, mechanical stresses especially at the particle edge can create cracks on the SEI layer leading to an increased SEI formation current. Then from

mechanical modelling of the electrode behaviour, mechanical integrity of bonds between particles have been investigated.

Most of approaches so far are given for repeated and cyclic solicitations. However, such solicitations are not realistic in automotive applications. As a consequence, an approach considering instantaneous contribution to material degradation have been used.

- **SEI cracking**

As stresses occurs into the particles, stress at the outer edge is directly impacting the SEI stability. These stresses can create cracks leading to increased SEI formation. To assess the impact of such cracks, the derivative of concentration induced stresses at the particle edge is evaluated. SEI cracks will increase the SEI formation rate leading to higher losses of Lithium inventory while not creating a thicker SEI thickness which reduces the kinetics of SEI layer formation.

- **Loss of active material**

Due to stress building up in the electrode composite due to material swelling, loss of electronic conductivity between active material and collector may occur leading to loss of active material. As for the SEI cracking, this loss rate is proportional to the stress variation rate inside the electrode. In an initial implementation of the model, the maximum hydrostatic stress in particles has been used.

## 2.5.2 SPM-e model results

Three main analyses have been performed with the SPM-e model. First the simulation of the formation cycle has been performed. With the resulting parameter cell, the behaviour of the SPM-e model has been compared to experimental measurement of the nominal behaviour of the battery cell. Then aging simulation were performed.

### Formation modelling

To initiate battery state after manufacturing, the formation cycle has been modelled. To perform such a simulation, the geometric parameters as well as the material parameters are set according to nominal calibration. The initial insertion rate of the positive electrode is set to a value close to 1 to represent a fully lithiated electrode, and the insertion rates for the two negative materials are set to 0, and the initial thickness of SEI layers of both materials are set to 0. Then the formation profile is imposed to the model, and the initial performances of the cell are estimated using a specific check up protocol. For the model, the estimated capacity of the cell is 5.28 Ah and its internal resistance is 22 m $\Omega$ . Such values are consistent with experimental values where the mean capacity was estimated to 5.2 Ah and the mean internal resistance 18.4 m $\Omega$   $\pm$  2 m $\Omega$ .

### Nominal results

Once the formation has been performed, some of the final values of the model should be used as initial values to perform further simulation, such as the initial insertion rate, the initial SEI thickness and the initial losses of active material in both negative and positive electrode, which derived from the formation itself. The result of the model can then be compared to experimental tests performed at IFPEN. Three types of tests have been performed for the validation: C-rate cycles, Hybrid Pulse Power Characterization (HPPC) cycles and road cycles, at various temperature.

Figure 18 shows the voltage response of the model to discharges rates at 25°C. The results are in good agreement with the experimental behaviour.

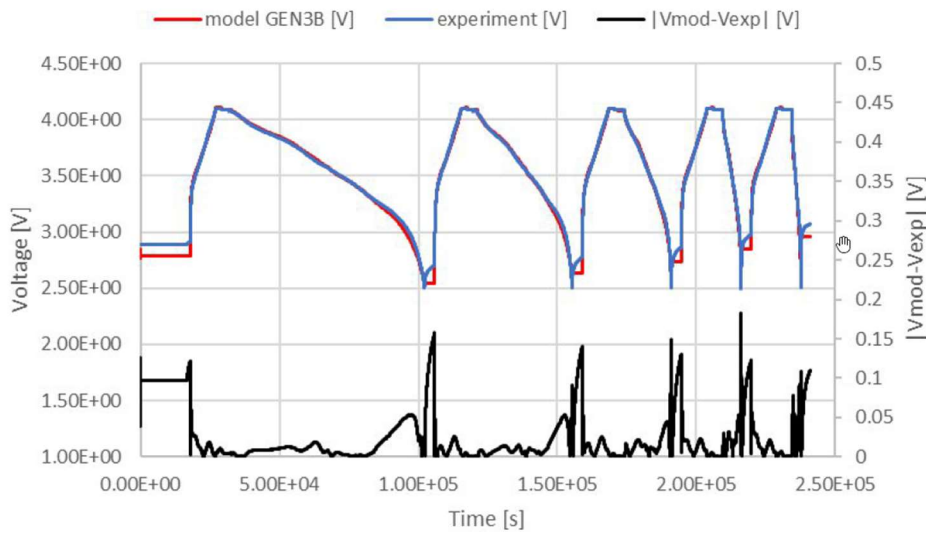


Figure 18: Comparizon between model and experiment on a C-rate discharge cycle at 25°C

Figure 19 presents the voltage response of the model on a few pulse trains of an HPPC protocol at 40°C. The results show again a good agreement with the experimental behaviour, with a good dynamic response of the model for short pulses, in charge or in discharge and for different current values.

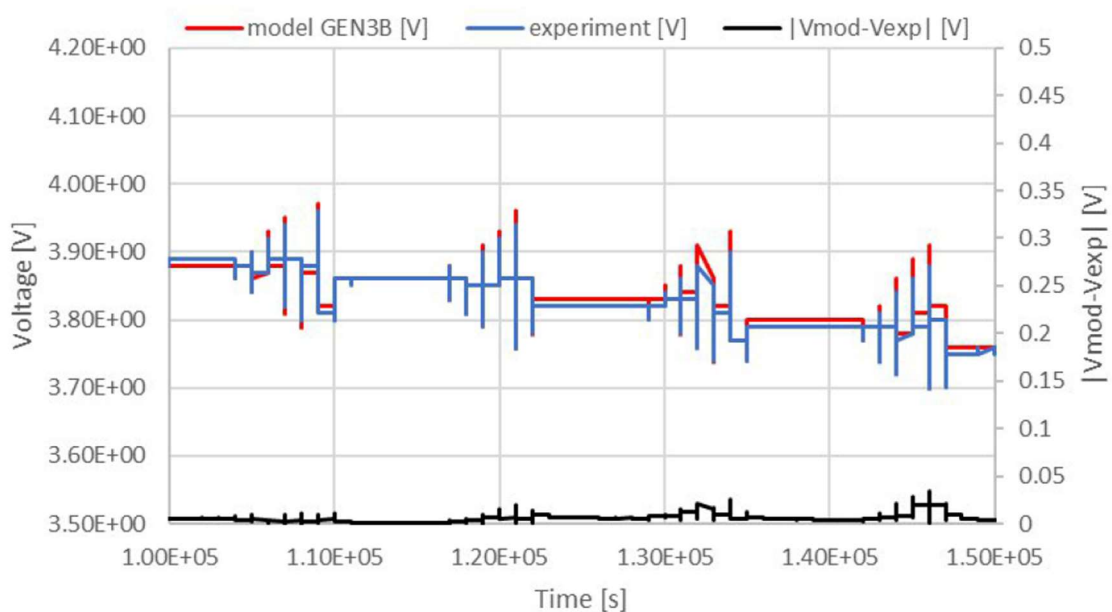


Figure 19: Comparizon between model and experiment on a window of a HPPC cycle at 40°C

The thermal response of the model has also been validated against experimental results.

### Simulation of aging

Aging behaviour of the model can be assessed under both calendar and cycling aging. Figure 20 presents an example of comparison of model capacity loss with experimental results of a cell stored at 45°C. The cell lost 10.5% capacity over 100 days and the shape of the curve is representative of SEI formation capacity loss which is expected in such conditions. The total calculation time to simulate the 100 days of storage is only a few minutes. A dedicated analysis shows that in this case, the main aging mechanism involved dis simple SEI formation, the other mechanisms being negligible.

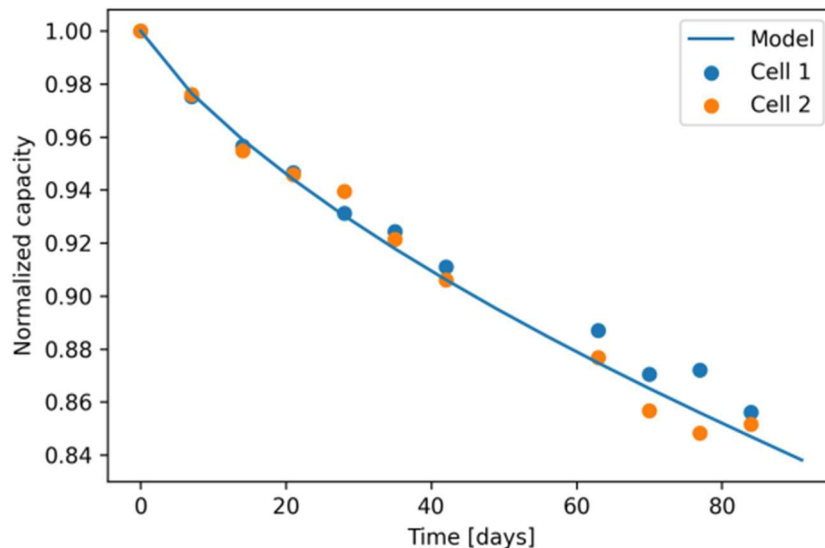


Figure 20: normalized capacity loss during calendar aging compared to experimental data

### 2.5.3 Thermal runaway model description

The thermal runaway modelling consists in an electrical equivalent circuit model calibrated thanks to the electrochemical model. The battery model comprises in addition to the electrical equivalent circuit a thermochemical model able to represent the main thermal runaway reactions occurring in the cell. Finally, this model is coupled to a thermal model comprising not only the behaviour of the cell but also the behaviour of the jig.

A specific current profile has been applied to the SPM-e model. This profile is a succession of 3 cycles of charge and discharge at constant current with rests between each current, followed by a HPPC discharge. The voltage and temperature computed by the SPM-e model are then stored

in datafiles, and a specific electro-thermal battery identification tool is used to extract the parameters of the equivalent electric circuit model present in Figure 21.

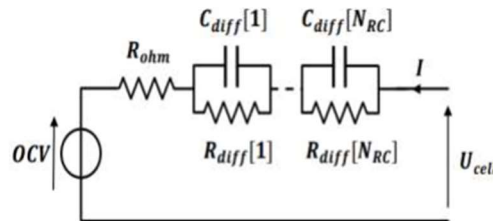


**Figure 21: equivalent circuit model of a battery cell**

Figure 22 presents a comparison of the voltage and temperature of the equivalent circuit model with the results of the SPME-e model: During constant current solicitation (from 0 to 1800 min) the voltage of the equivalent circuit model is in good agreement with the SPME-e model output except for the discharge final voltage value. During pulsed discharge, the discharge phase are very well reproduced. A slight discrepancy between the models voltages appears during charge phase. This come from the fact that the hysteresis between charge is not considered here as the focus is on discharge.

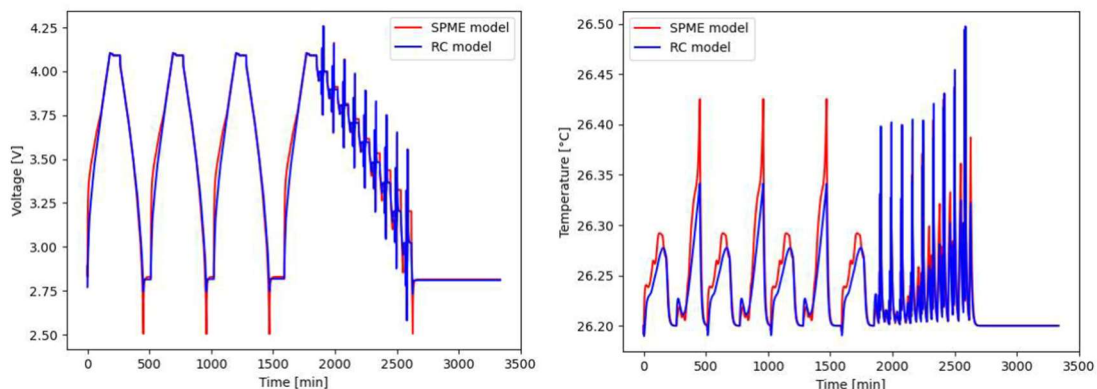


**Figure 22: comparizon of the equivalence circuit model (RC) with the SPM-e model**

The thermal runaway model is implemented in the equivalent circuit model. The model consider the energy generated by different reactions: the passivation layer degradation, the negative and positive electrode degradations, the venting of the gas, the self discharge and the electrolyte degradation.

### 2.5.4 Thermal runaway model results

Accelerating Rate Calorimeter (ARC) test has been performed, and a model of the test jig including all the thermal exchanges in the calorimeter has been developed: convection between calorimeter wall and air and between air and solid elements (cell and holder), conduction between holder and cell and radiation between all elements.

The self-heating temperature raise recorded experimentally is then used to calibrate the thermal runaway model. Figure 23 shows that the calibrated model satisfactorily reproduce the self-heating temperature rise until 400°C. At the very beginning of thermal runaway (before 2200min) the temperature is slightly overestimated by the model. Nevertheless, the experimental slope break around 2500min is well predicted.

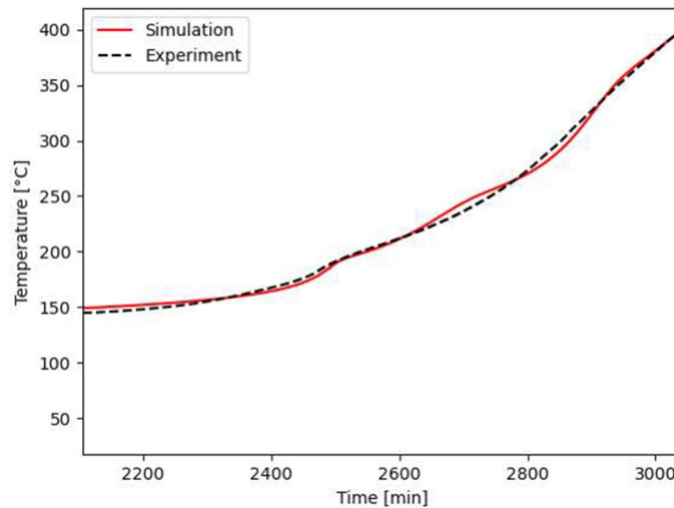


Figure 23: Modeled and experimental cell temperature comparison during self-heating phase

## 2.6 3D macro-homogeneous approach

In order to evaluate the impact of inhomogeneities inside the cell, an extension of the porous electrode modelling capabilities of Simcenter STAR-CCM+ for the simulation of Gen3b batteries has been developed. The lithium transport in the active material was modified such that stress-driven diffusion is accounted for. In addition to that, various aging models developed for the SPM-e model have been adapted and implemented: Mechanical degradation of both electrodes, growth of the Solid-Electrolyte Interphase, lithium plating, and cathode dissolution.

### 2.6.1 3D Cell Design in Simcenter STAR-CCM+

In order to support the integration of the 3D macro-homogeneous models derived from the project and to allow for a comfortable and productive user experience, a specific tool dedicated at cell design was developed in Simcenter STAR-CCM+ in parallel to the project.

It is a new unique capability to design lithium-ion battery cells in 3D.

The solution is based out on a template simulation file which means a pre-setup model to accelerate the pre-processing steps and let the user focusing only on the cell input data.

The solution allows for the design of Lithium-ion cells in full 3D, with geometrically resolved electrode layers, separators and tabs, something unseen on the market yet.

It also provides high accuracy models with 3D solution of the electrochemical behaviour of the cell thanks to an enhanced physics-based model from the initial Newman-Doyle-Fuller formulation described in more details in chapter 2.6.2.

The workflow within the simulation template, leverages existing and new features for a customized and tailored workflow for cell designers, with industry-standard terminology and units.

It has a simplified meshing setup in a few inputs and clicks and supports dedicated industry-standard post-processing to facilitate the analysis from the simulation results

The capability is driven by 3 simulation templates, one for each cell shapes: stack, cylindrical or prismatic wound, which are the industry standards

Finally, as with templates, these are simulation examples and the user is free to edit the template to further customize it to their needs.

This capability will be made publicly available to customers at the end of October 2023.

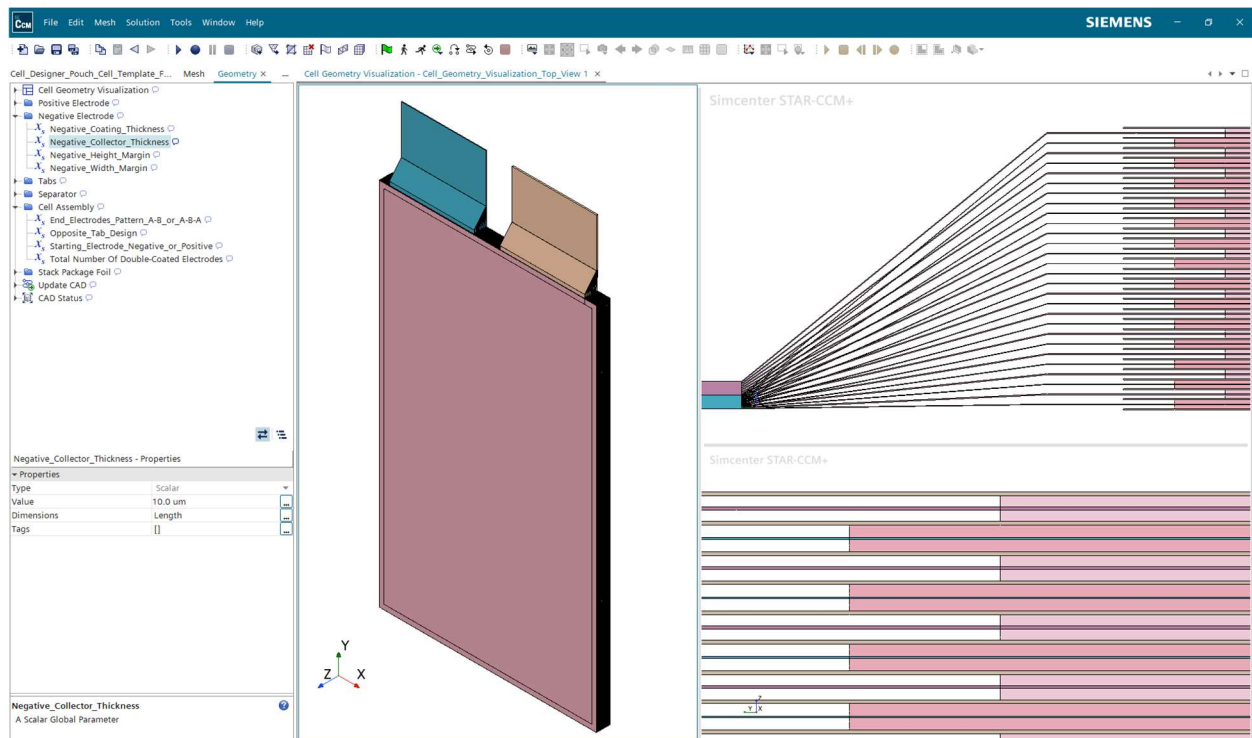


Figure 24: Interface of the 3D cell design simulation template in Simcenter STAR-CCM+

## 2.6.2 3D Cell Modeling approach

Simcenter STAR-CCM+ contains its own implementation of the Doyle-Fuller-Newman model [6], which serves as basis of the developments for Modalis2. The model employs a two steps approach (Figure 25). The macro-homogeneous domain is characterized by the porosity, the tortuosity, and the volume fractions and the specific surface area of each solid phase (e.g., the active material, the binder, the conductive aid, or the products of side reactions), but none of their microstructural features are explicitly resolved. At the microscale, the active material is represented by idealized spherical particles. To describe lithium intercalation and diffusion within a particle, a

1D transport problem is solved. The coupling between macro and microscale is achieved by appropriate boundary conditions. The prescribed fluxes at the particle boundaries are linked to sources/sinks in the macro-homogeneous domain via the specific surface area, defined as the surface of a porous phase per unit volume. The particle surface flux driven by the intercalation reaction is governed by standard Butler-Volmer reaction kinetics.

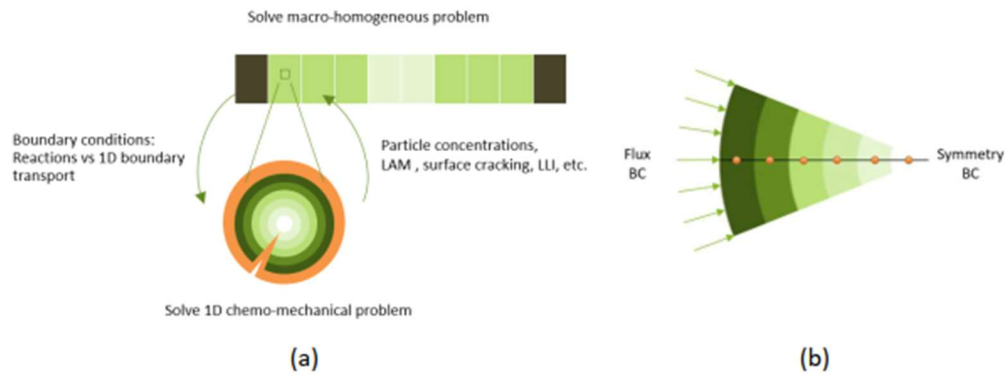


Figure 25: Scale bridging in the sub-grid particle model(a) 1D discretization of the particle model(b)

### Micro-scale modelling of volumetric expansion effects

Similarly to the work done for the SPM-e model, the mechanical at particle level has been implemented, based on the analytical solution for the radial and tangential stresses within the particle due to the presence of the intercalated lithium from [1].

### Macro-scale modeling of volumetric expansion effects

The volumetric expansion and its effect on the cell thickness are calculated in two steps. First, the thermo-electro-chemical macro-homogenous problem is solved using the finite volume (FV) method. Next, the average particle concentration field is imported to a finite element (FE) simulation and mapped onto the FE-mesh. Figure 26(a) shows the overlay of FV and FE discretization, Figure 26(b) shows the FE-mesh only. As pointed out above, electrode swelling and thermal expansion are very similar from a modelling perspective. Therefore, the concentration field is scaled and added to the temperature field. In the second simulation step, the thermo-mechanically coupled problem is solved.

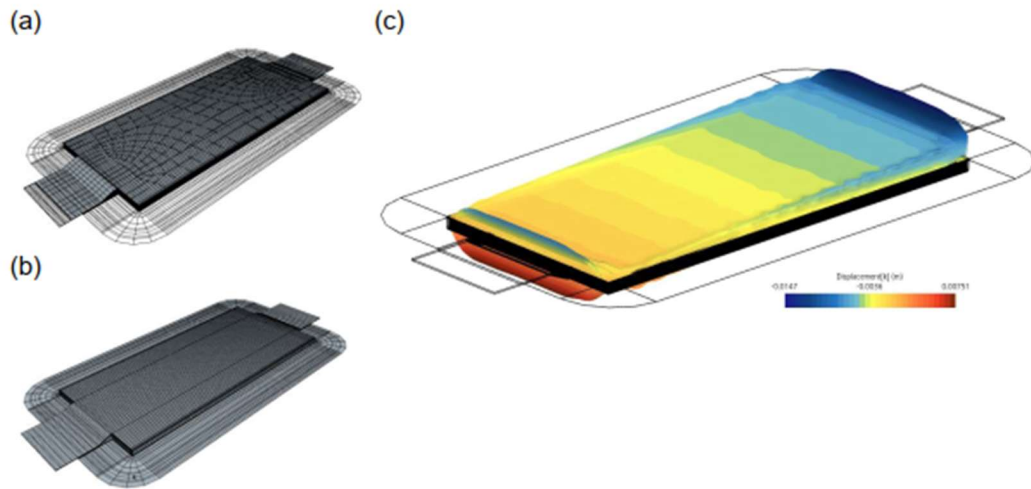


**Figure 26: V-FE discretization overlay (a) FE discretization (b) Swollen configuration of the thermo-mechanical FE simulation (c)**

### Aging modeling

The physics based models of battery aging developed in the SPM-e model were adapted for their implementation in Simcenter Star-CCM+.

- **Solid-Electrolyte Interphase growth**

In the SPM-e model, a transport limited model for the SEI growth is implemented. In this model, the solvent concentration is spatially resolved in the SEI layer: The solvent concentration at the electrolyte-SEI interface is assumed to be different from its concentration at the SEI-particle interface. To compute the concentration at the inner interface, another 1D diffusion problem needs to be solved. Given the solvent concentration at the SEI-particle interface, the reaction current is evaluated using well known reaction kinetics of Tafel or Butler-Volmer type. However, the simpler approach of kinetically limited growth has been chosen for the implementation in Star-CCM+. This approach directly uses the bulk solvent concentration to compute the reaction current. To compensate for the limited solvent availability at the reaction site due to slow diffusion through the SEI layer, the specific reaction current is chosen sufficiently low and may even depend on the thickness of the SEI layer.

To this end, the Solid-Electrolyte Interphase model has been added to the Simcenter STAR-CCM+ prototype which discloses a porous phase as a thin surface film of on a particle phase. It has several roles:

- Providing the SEI material with its properties like density, ionic conductivity, elemental composition, etc.
- Making the SEI material available as reactant / product in electrochemical reactions.
- Providing geometrical information in a sense that it points to the substrate particle phase. This is important when multiple active particle phases are present in the same electrode

and allows to accumulate a total reaction current. This is required for the correct calculation of the ohmic drop

- across the SEI thickness.
- Updating the film thickness.

- **Lithium plating**

Like the growth of the solid-electrolyte interphase, Li plating (LiP) is caused by a parasitic side reaction. As before, the Solid-Electrolyte Interphase model is used to make the Li-metal available as reactant / product but the ionic conductivity is set to zero. Again, the Solid-Electrolyte Interphase model takes care that the side reaction current is correctly accumulated into the total reaction current of the corresponding particle-film system.

- **Loss of active material**

To model the loss of active material (LAM), the Sub-Grid Particle Aging model has been implemented. It contains two sub mechanisms which can individually be enabled: mechanical degradation and dissolution of the particle phase.

### 2.6.3 3D Cell Modelling results

The capability to investigate the non-uniform aging in Gen3B cells is demonstrated in this part. A specific cycle is applied 10 times to the stack presented in Figure 26, which consists in a CC/CV charging at 2C/4.2V until 95% SOC, a rest during 200s, a CC discharging at 2C until 60% SOC and 200s of rest.

Figure 27 presents the results of the aging models in-plane and in-thickness directions.

In-plane, the thermal boundary conditions are such that the highest temperatures are observed at the center of the battery cell, where the temperature-dependency of multiple material parameters leads to increased SEI growth rates. LAM is pronounced close to the battery tabs, where the highest stress change rates are observed.

As expected, in-thickness SEI growth and LAM are highest near the separator. The operation conditions are such that the Li-metal, with initially specified homogeneous profile, is dissolved faster than it is deposited, especially close to the separator.

CONFIDENTIAL until public release by the MODALIS<sup>2</sup> project consortium

Simcenter STAR-CCM+

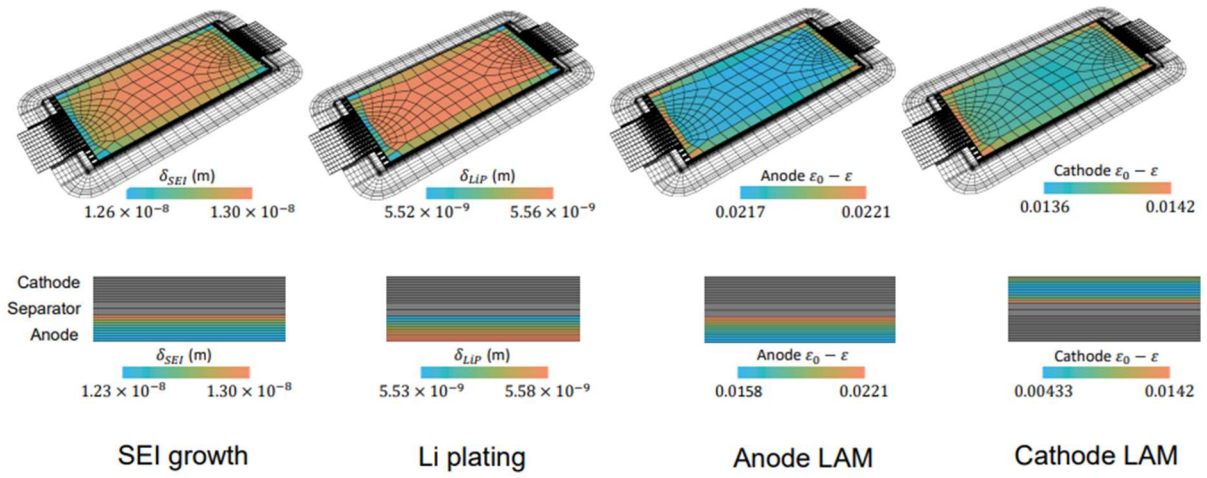


Figure 27: Heterogeneous aging in cathode and anode: in-plane and in thickness direction

### 3 Gen4 simulation tool chain

#### 3.1 Gen4 toolchain overview

The tools and methods used to represent Gen3b cells have also been applied to Gen4 cells, especially focusing on the behaviour at the interfaces. Investigations were performed in a total of 4 modelling scales:

Atomic-scale quantum-mechanical simulations were performed of the anode and electrolyte bulk material, as well as for the study of the interfaces between the different materials.

At mesoscopic scales, Phase field models were used to investigate the dendrite growth mechanisms and FEM was done to evaluate the impact of mechanics on electrode stability.

At cell level, a 1D SPM-e model has been adapted to represent Gen 4 batteries behaviour.

A prototype of 3D model of cell has also been developed

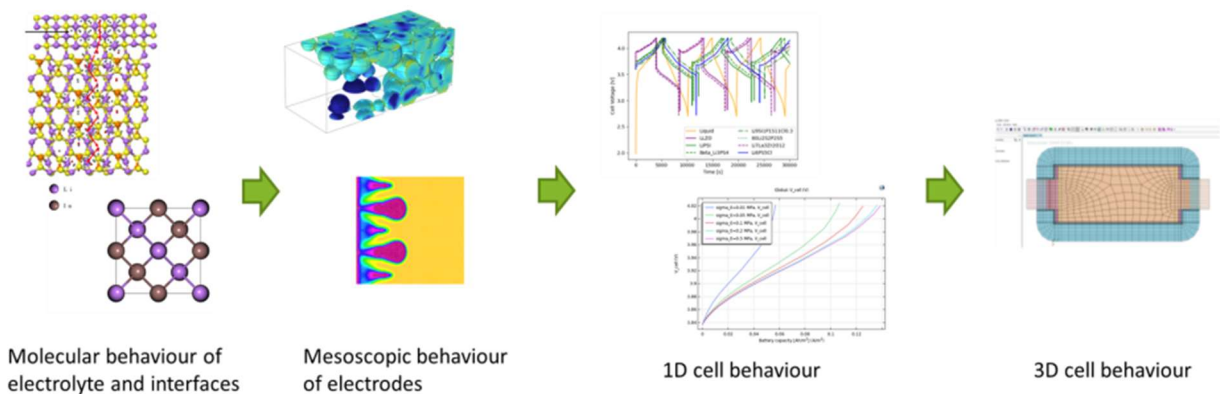


**Figure 28: Gen4 toolchain overview**

The studied cell is a prototype pressure cell composed of NMC 811 coated positive electrodes and Li-In negative electrodes and Sulfide powder for the Solide electrolyte layer. The negative electrode has been deposited on 10 μm thick copper foil and the positive ink on 15 μm thick aluminum foil.

## 3.2 Atomistic modelling

Atomic-scale quantum-mechanical simulations of the anode and electrolyte bulk materials have been performed.

The structure of seven Li/In mixtures as potential anode materials was studied, with the aim of outlining a possible partition and ideal mixture, and investigating the role of In in the mechanical properties of the material.

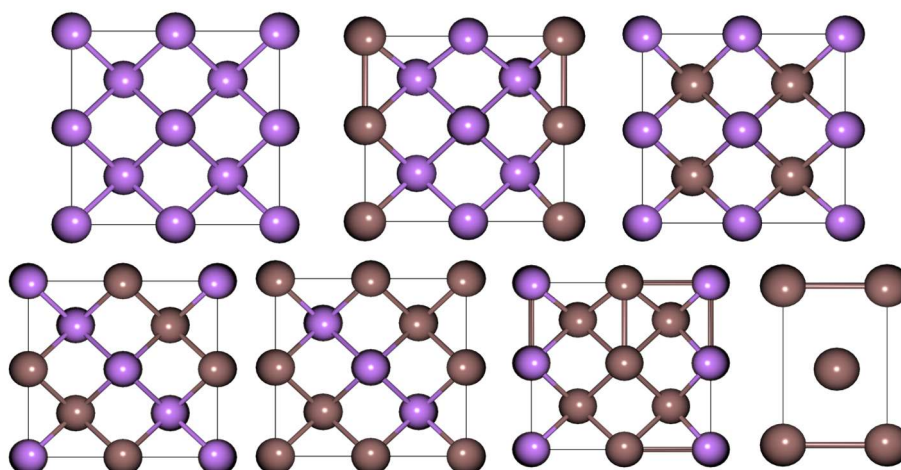


**Figure 29:** *Li<sub>x</sub>In stoichiometries investigated in this study. From top left: Li, Li<sub>3</sub>In, Li<sub>1</sub>In, Li<sub>0.45</sub>In, Li<sub>0.4</sub>In, Li<sub>0.3</sub>In,*

For pure Li, the data is consistent with previous literature across all mechanical parameters. For pure In, the same is true for the Bulk modulus, but deviates significantly from previous reports for Shear modulus, Young modulus and Poisson's ratio. The reason for this inconsistency might be found in the small size of the employed In unit cell. While larger-scale calculations are likely to solve this issue, these have not been performed because, for the scope and objective of the present study, the consistency of Bulk moduli was considered sufficient. For the intermediate phases, no literature reference could be found; however, the Bulk moduli are found to be internally consistent and comparable to literature data for similar alloys.

Trends in their mechanical properties as a function of Li content were identified. Of the seven investigated bulk structures, however, only In, Li, and LiIn were used for further investigation of the surface and reactivity of these anodic materials.

The bulk Li<sub>6</sub>PS<sub>5</sub>Cl argyrodite solid electrolyte was studied revealing a low-temperature symmetry breaking in the crystalline structure, so far unknown in the literature. Evidence of the correctness of such finding against literature experimental data was provided. Additionally, the thermal expansion and elastic properties of the solid were studied in detail through a quasi-harmonic approximation. A similar study was carried out for another solid-state electrolyte,  $\beta$ -Li<sub>3</sub>PS<sub>4</sub> by simulating the details of its structural and electronic features.

Investigation of material interfaces at the atomic and particle scale has also been performed. During the charge and discharge process, the morphological changes at the interface between materials are often the source of much of the stress and failures associated with novel LIB materials. The investigation of the properties of these interactions, either through the study of the individual interfaces or through direct observation of the chemical and mechanical changes associated with lithium diffusion, is key to the development of commercially viable ASSBs.

The stability of  $\text{Li}_6\text{PS}_5\text{Cl}$  argyrodite solid electrolyte surfaces is investigated and a Wulff plot for the material is constructed (Figure 30). The plot is polar, due to the lack of vertical symmetry in the slab models, with the sole exception of the (110) surface. The different terminations are also analysed, predicting a potential passivating feature of the (001) and (111) surfaces, due to the electronically insulating but ionically conducting precursors exposed through these cuts, though phase transitions to  $\text{Li}_2\text{S}$  and  $\text{LiCl}$  SEI components might hinder this possibility.

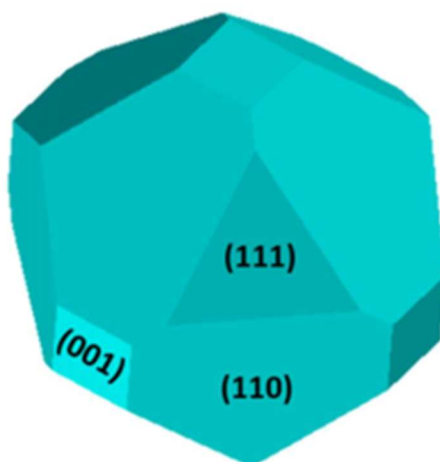


**Figure 30: Wulff's polar plot for cubic symmetry of argyrodite**

Similarly, surface stability is extensively investigated for the  $\text{Li}_3\text{PS}_4$  sulphur solid electrolyte system. Based on the calculated surface formation energies and Gibbs free energies, the (100) surface resulted as the most stable, followed by (210), (011), and (010). In addition, the (100) and (210) films showed interesting features such as good mechanical and thermodynamic stability; a high concentration, and good mobility of Li ions, and a potentially small lattice mismatch with materials such as  $\text{Li}_2\text{S}$ , widely used as a passivator in lithium technology. The (010) structure presents original characteristics, such as peculiar surface states and a net dipole moment along the non-periodic z-axis, which could eventually increase the diffusion rate of the lithium ions. Finally, Wulff's theory was applied to derive the shapes of possible nanocrystals. As proof, it has been verified that the extra-stabilization of both the (100) and (011) surfaces, done by hand, leads to nanoplates very similar to those synthesized experimentally (Figure 31).

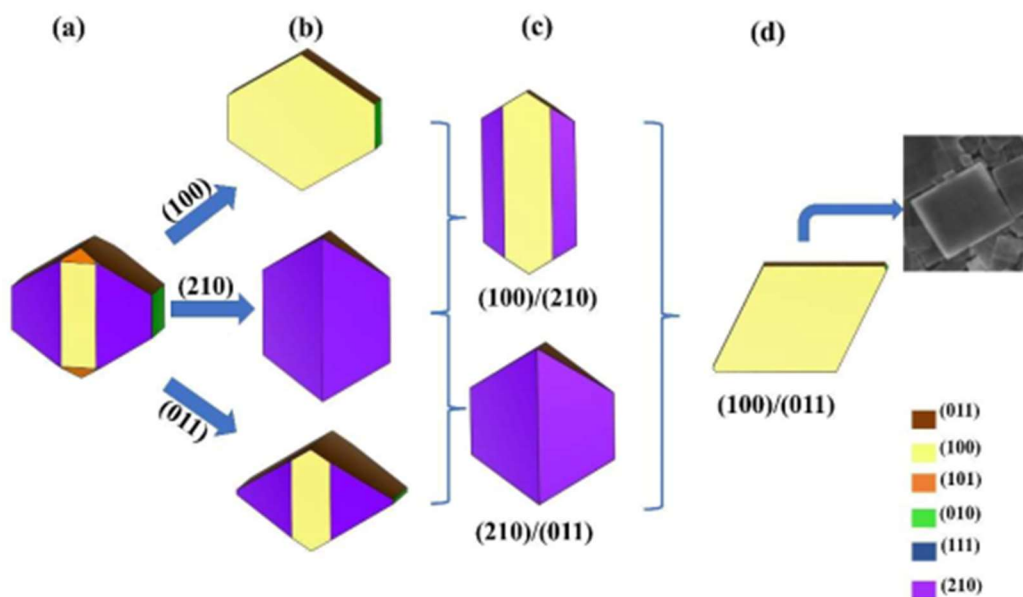


**Figure 31: Different morphologies of  $\beta$ -Li<sub>3</sub>PS<sub>4</sub> nanocrystals obtained by varying the relative stability of the various surfaces**

Based on this, the interface formed between the most stable surface of Li<sub>3</sub>PS<sub>4</sub>, (100), and the (110) surface of Li-anode was analyzed. As discussed in some previous works, when these two materials are put in contact, many structural defects are formed, and the Li<sub>2</sub>S begins to be formed in the first layers of the interface. In parallel, P atoms from the LPS surface migrate towards the Li-anode and form Li<sub>3</sub>P. Therefore, this interface becomes unfeasible for direct application in Li-ion batteries, requiring the use of a passivating material to inhibit this chemical reaction between Li/LPS. In this way, we proposed the Li<sub>2</sub>S surface (110) as a passivating coating material, which presented good adhesion energy with both Li and LPS surfaces, in addition to presenting the minimum modification in the electronic properties, which guarantees the continuity of the conductivity ionic. Furthermore, the negative adhesion energies suggest that such interfaces, Li/Li<sub>2</sub>S and Li<sub>2</sub>S/LPS, are formed spontaneously and with low strain energy. This study showed the need to use the surface (110) of Li<sub>2</sub>S as a passivating material to avoid the formation of Li dendrites, without impairing the migration of Li ions and the ionic conductivity of the LPS.

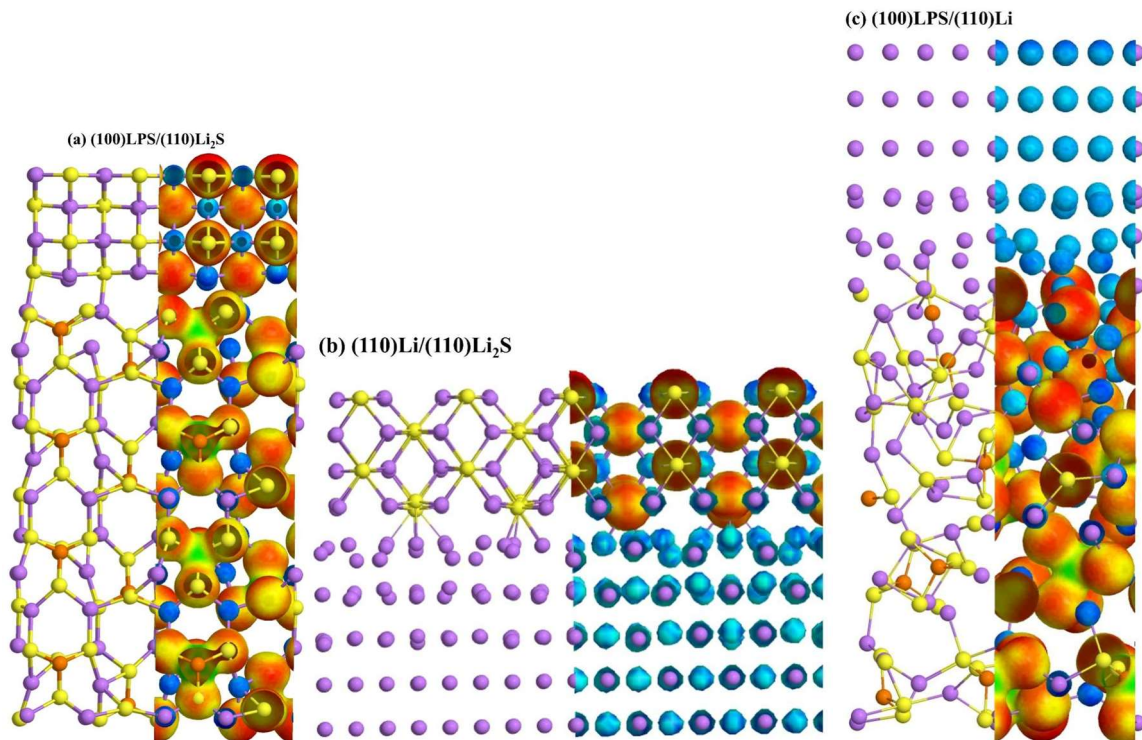


Figure 32: Final optimized interfaces and their charge distribution on the isodensity surface: (a) (100)LPS/(110)Li<sub>2</sub>S, (b) (110)Li<sub>2</sub>S/(110)Li-metal, and (c) (100)LPS/(110)Li-metal

### 3.3 Mesoscopic scale

#### 3.3.1 Dendritic growth modelling

In electrochemical simulation models, interfacial reactions with the motion of phase boundaries are complex for conventional approaches. The phase-field method seems an effective tool for bypassing the evolving complex geometry in conventional sharp inter-phase methods to simulate the dendrite growth potentially generating cracking in the electrolyte.

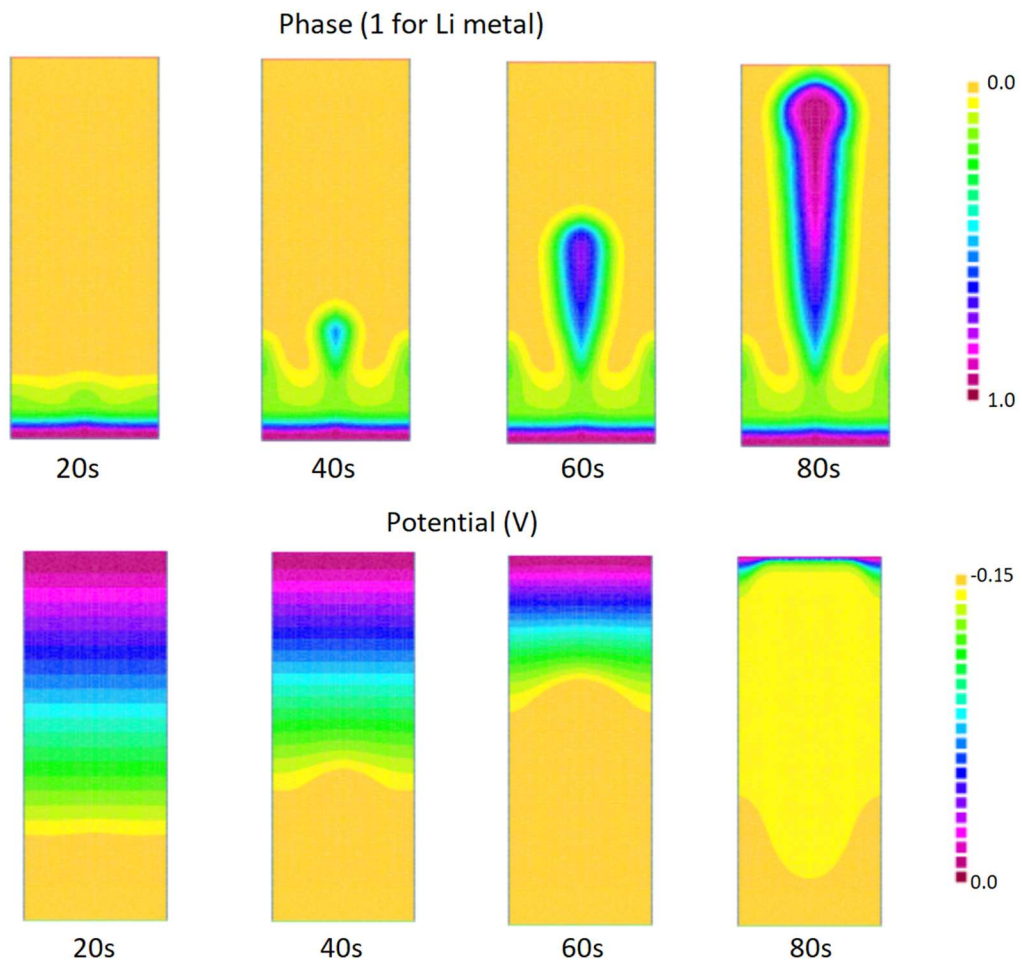
A phase field model prototype has been implemented using the multiphysics finite element software Freefem++ (see <https://freefem.org/>) in order to investigate the potentiality of the approach for dendritic growth prediction. The model makes the following assumptions, coming mainly from [12]:

- No granular structure from the electrolyte
- Mechanical behavior of the anode and electrode not considered
- Dendrite nucleation is supposed nucleated from a geometric protuberance at the electrode surface
- No electron trapping mechanism on internal defect surfaces is considered

An example of some calculation is presented in Figure 33. At the beginning of the computation, the phase field is set to 1 on the lower bound, and a difference of potential of 0.15V between the

upper and lower bounds is applied. The dendrite growth therefore starts and is simulated to represent the evolution of the three fields.

The evolution of the Li metal front through the electrolyte with  $Li^+$  normalized concentration and potential can be observed. The formation of 1 mm square of Li metal requires an amount of  $Li^+$  significantly higher than what is initially available for such a surface. The dendrite nucleation and growth therefore consume a significant amount of  $Li^+$  and lead to a decrease of  $Li^+$  concentration. The growth of the dendritic is only possible because a continuous diffusion of  $Li^+$  from the upper bound to the lower parts of the model. Therefore, the dendritic growth is clearly driven to the upper bound and to available  $Li^+$  ions. The dendrite growth also significantly affects the potential in the modelled media because of Li metal high conductivity compared to the initial one. The last state shown in Figure 33 could be considered as the appearing of a short-circuit.



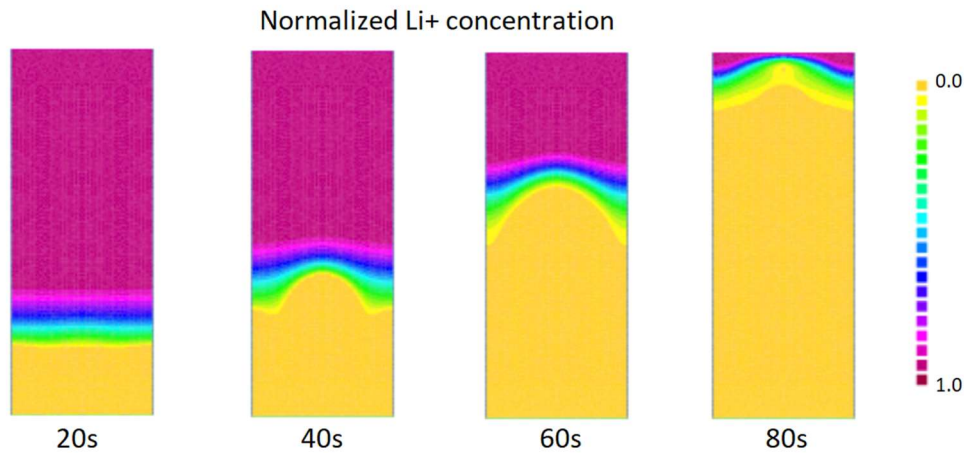


Figure 33: Snapshots of Li metal  $\xi$ , electric potential  $\phi$  and concentration of ion  $Li^+$  at various evolution times

These results demonstrate the potential of the prototype model to represent the onset and growth of Li metal dendrites in battery. The present study is not exhaustive, and the modelling tool could be used to help in the understanding of the link between defects, dendrites onset and growth, media properties and loading.

### 3.3.2 3D mechanical modelling of the Gen4 cell

A microscale level model of a representative portion of a Gen4 cell model was developed in order to predict the performance of the cell as a function of the cathode structure and to provide guidelines for improving the electrode design. The first part of the work was dedicated to the development of a representative cathode geometry by implementing an in-house code using the Octave language. The positive electrode was constructed as an ensemble of spheres, representative of the active material (namely, NMC811) and the aggregates of a carbon-based conductive additive. For the sake of simplicity, the cell anode was modelled as an ideal lithium plate, whose thickness varies due to deposition and stripping of lithium during operation, separated from the cathode by a thick layer of solid electrolyte. The Solid Electrolyte was modelled as a continuous homogeneous medium, neglecting its original granulometry. The volume fractions of the cathode components, and the cathode and separator thicknesses were evaluated considering the data collected from the manufacturing process.

A representative box size was used to generate a geometry used in finite elements simulations in COMSOL Multiphysics to determine cell performance, in an automated way. The mechanical stress caused by the intercalation of lithium in the NMC and the deposition/stripping of lithium at the anode has been included in the model, contributing to the cell performance (stress-induced diffusion within the NMC particles). Since coupling the mechanical model with the electrochemical and thermal phenomena in a time-dependent solver would be too computationally expensive, COMSOL was set up to evaluate the mechanical stress at regular time intervals and update the associated transfer properties.

Examples of the FEM model results can be seen in Figure 34. The evolution of hydrostatic pressure (black data) and normal stresses (red, green and yellow data) as a function of simulation time are presented in A. Initially compressed by the applied axial load of 395 MPa, the pressure decreases during charging due to the contraction of the NMC during the deintercalation of lithium. However, cracks and damage are likely to occur during operation due to the constant pressure of over 100 MPa applied to the active material. The pressure distribution in the NMC at the beginning of the simulation and at the end of the first charge at C/20 are presented respectively in B and C.

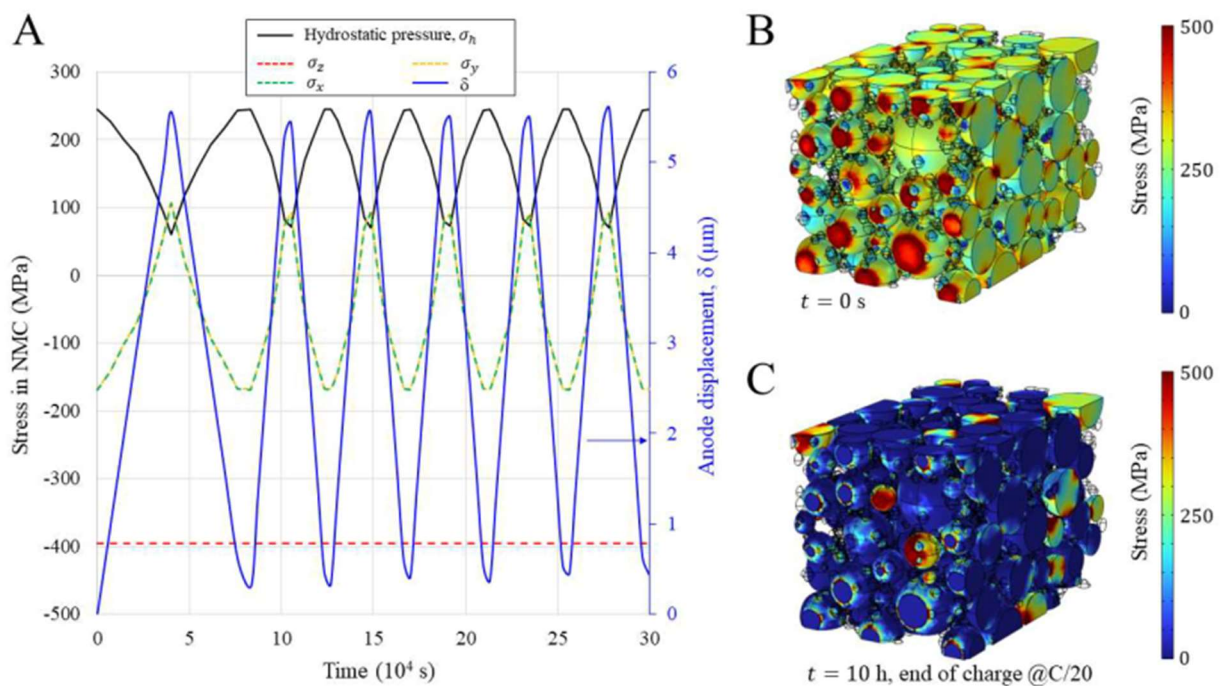


**Figure 34: Mechanical stresses and deformations.**

The analysis reported above shows the suitability of the proposed modelling approach to study and engineer the cathode microstructure in order to predict and optimize the resulting cell performance. The open-source software developed allows to generate and analyze geometries representative of real cells, allowing the evaluation of several crucial parameters (PSD, active material fraction, active surface, percolation of CB aggregates), which can be easily compared with their experimental counterparts, thus validating the generated microstructures.

The FEM simulations allow a comprehensive study of cell performance by coupling electrochemistry, mechanics and temperature distribution in a 3D-resolved model. The Gen4 cell studied reproduced the experimental performance with acceptable accuracy. Mechanical stresses and strains had a negligible effect on the transport phenomena considered, while the pressure distribution, often exceeding the 100 MPa threshold, indicates working conditions where the active material is likely to be damaged.

In perspective, future implementations of the model should address the impact of pressure-induced damage in hindering NMC transport properties (namely Li diffusion and intercalation, electrical conductivity), and quantitatively evaluate how shear stresses influence detachment at the NMC-SE interface and current collector.

### 3.4 Single Particle Model with Electrolyte

Following lower scale modelling, further development where needed in order to correctly model the behaviour of solid state batteries using a 1D modelling approach. Two main phenomena have been specifically addressed in this work. First of all, the ionic conduction within the electrolyte with a flat electrode on the left (the LiM or Li/In electrode) and the pressure dependency of current densities linked to the contact losses occurring between 2 solid materials. The 1D modelling approach was initially developed by [13] for thin film batteries. It has then been adapted to our studied system with a thin film negative electrode and a bulk electrode for the positive, and implemented in prototype version on the SPM-e model in Simcenter Amesim.

The parameters of the model have been adapted to represent the Gen3 cell of the project, based on the measurements performed in the project, adjusted with parameters from the literature [13][14] for diffusion and mechanical properties. Figure 35 presents a comparison of the model results with experiments for a HPPC test. On most part of the cycle, the model is in good adequation with the experiments, with an error lower than 50mV. Higher error can be observed at the end of the charge. This is probably due to a non-linear behaviour of Li-In. Further investigation on this behaviour would be needed to adapt the model and improve his representativity.

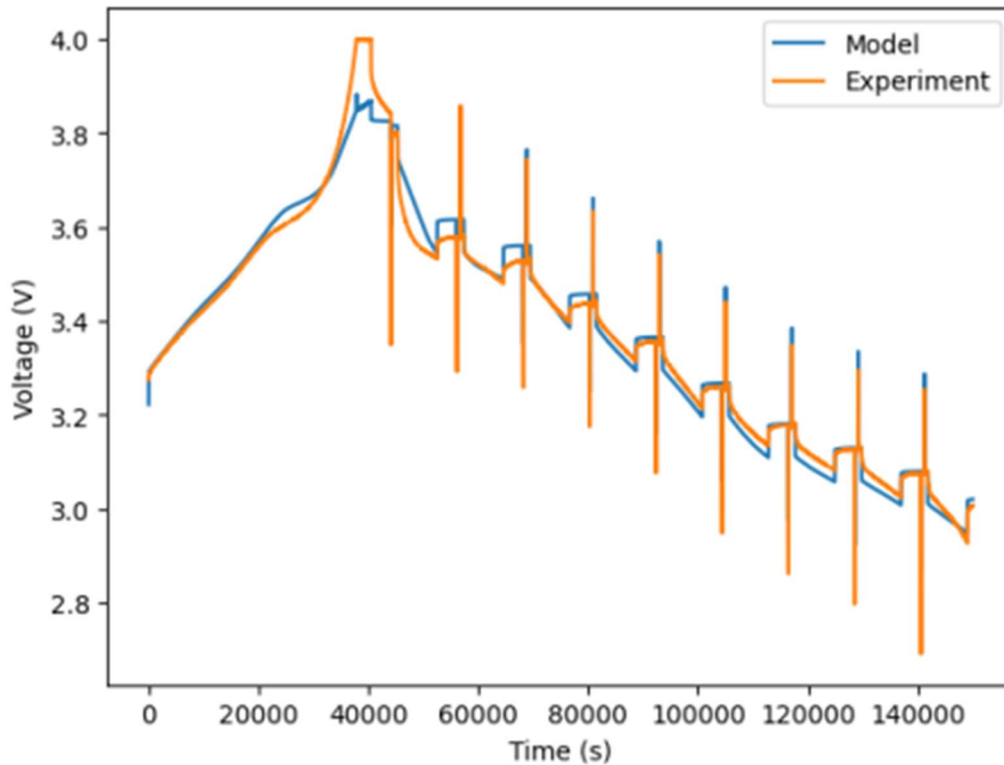


**Figure 35: comparizon of model and experiments on HPPC tests**

Similarly, C-rates have been performed on the model, from C/20 to C/2, showing strong electrolyte transport limitation at C/2, and numerical issues for higher C rates. Further development on the SPM-e model are needed to better handle high C-rates.

### 3.5 3D macro-homogeneous approach

A prototype simulator for Gen4 has been developed in Simcenter Star-CCM+. Due to certain limitations, instead of a negative flat electrode, both electrodes are modeled as bulk-type. The particle radius of the negative electrode was chosen such that the unresolved interface area of the porous electrode is equivalent to the interface of a corresponding flat electrode. The diffusivity of the Solid Electrolyte in the negative electrode region was increased artificially. The setup has focused on the physics modelling and for simplicity, only a thin slab geometry has been used so far, which basically resembles a 1D case. However, Simcenter STAR-CCM+ still solves the balance equations in three dimensions. The described physics setup can be almost identically transferred to more complex geometries.

Typical results are presented below in Figure 36 and Figure 37. The difference between both figures is the description of the elastic contact. In the first figure, the applied pressure is directly used, however this does not take swelling and shrinking effects into account and the required pressure is underestimated. The second figure uses the hydrostatic, which depends on the concentration of the intercalated lithium. A significantly higher pressure is required to guarantee a

sufficiently good contact between SE and AM. This is due to the shrinking of the active material during to deintercalation, which effectively lowers the pressure. This is in line with the findings of DEL2.5, reporting that the hydrostatic pressure changes with the average cell SOC. For the low C1/10 charge/discharge rate, the effect of contact imperfections is barely visible in Figure 37.

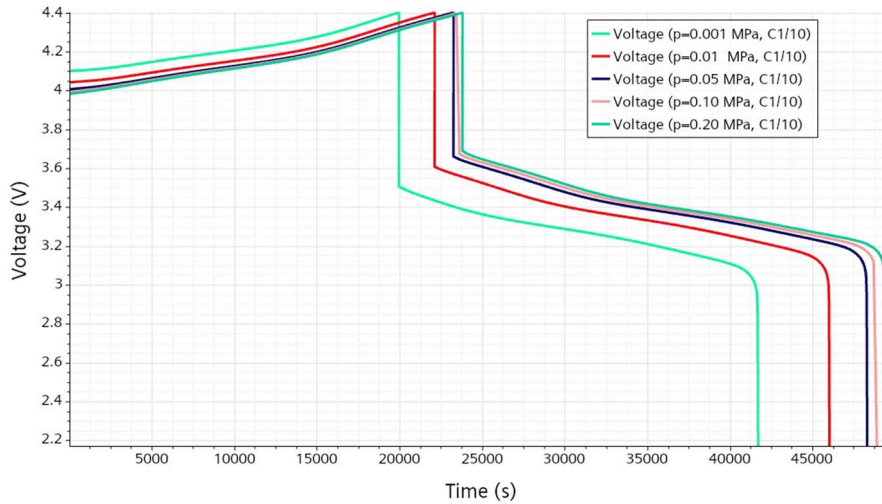


**Figure 36:** Charge-Discharge cycle for Gen4 batteries with varying prescribed pressure  $p^{pfs}$ . The prescribed pressure is used to describe the contact factor,  $\gamma$ .

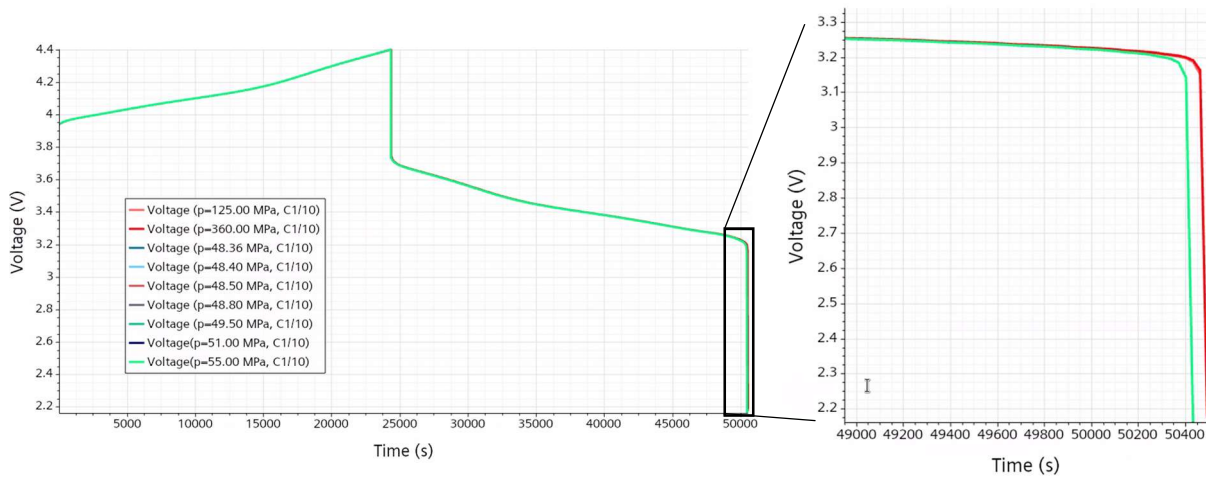


**Figure 37** Charge-Discharge cycle for Gen4 batteries with varying prescribed pressure  $p^{pfs}$ . The macro-homogeneous hydrostatic pressure is used to describe the contact factor,  $\gamma$ .

## 4 Conclusion and Perspectives

This document described in the detail the full simulation toolchain implemented in the MODALIS<sup>2</sup> project for Gen 3b batteries. A total of five modeling scales were developed, ranging from ab-initio description of the Si-based active material to electrochemical modeling of cell ageing, with a focus on cooperative model design. Models were used in conjunction with experiments to elaborate anode-wide and cell-wide models of the electrochemical performance of the cell, providing additional input for some of the models involved and validating the overall project design.

Similar models have been developed during the project for Gen 4 batteries, focusing on surface stability and lithium dynamics through solid/solid interfaces, and volumetric expansion model of cells. The validation of these models and their integration in a complete toolchain is still ongoing at the present stage.